Cosmology from the forthcoming Euclid Galaxy Clustering measurements

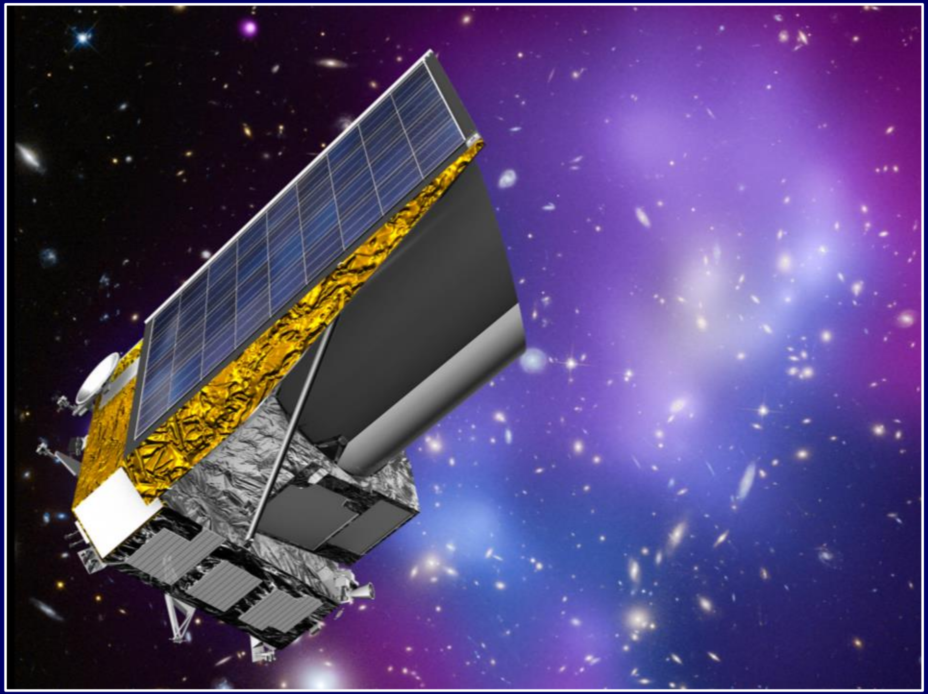

Carmelita Carbone (for the Euclid Consortium)

INAF Istituto Nazionale di Astrofisica
National Institute for Astrophysics
Istituto di Astrofisica Spaziale e Fisica cosmica di Milano

Dark Energy: from fundamental Theories to Observations (and back)
INFN-LNF, 11–15 September 2023, Frascati, Rome

Contributors (results, figure, slides, discussions…)

- Y. Mellier & the *Euclid Consortium* (all Euclid material shown on behalf of the EC)
- Many thanks to Guzzo (especially), Granett, Cuillandre, Hudelot, Fosalba, Sefusatti, Serrano, etc…

Unveiling dark energy and gravity with the Euclid double approach to the dark sector

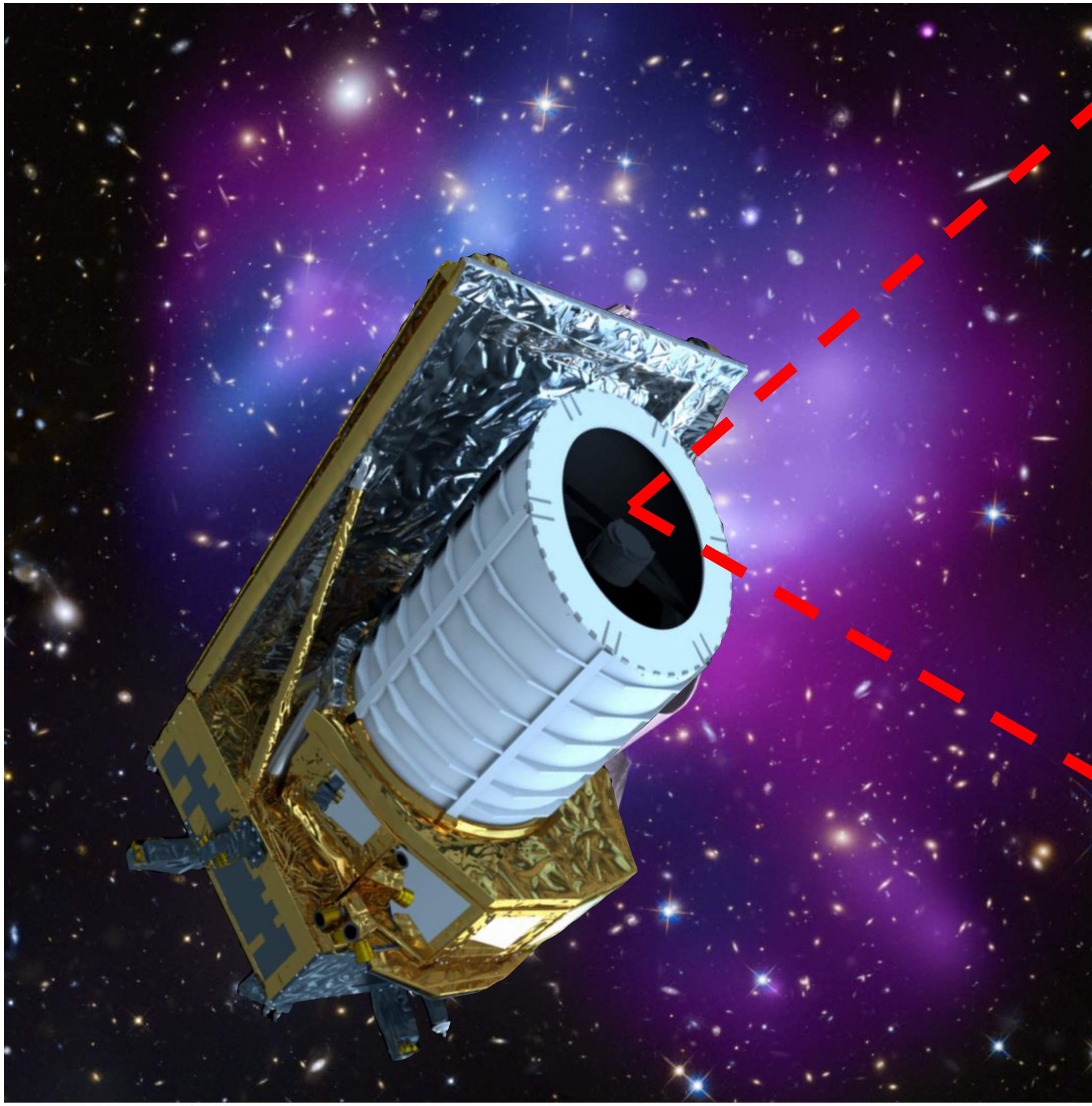

An artist view of the Euclid Satellite – © ESA

Weak lensing (z_s=1)

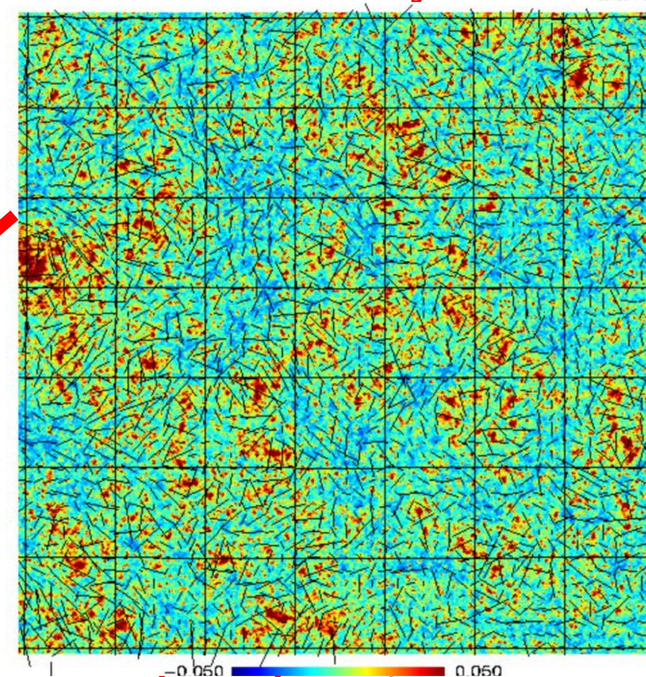

Galaxy Clustering

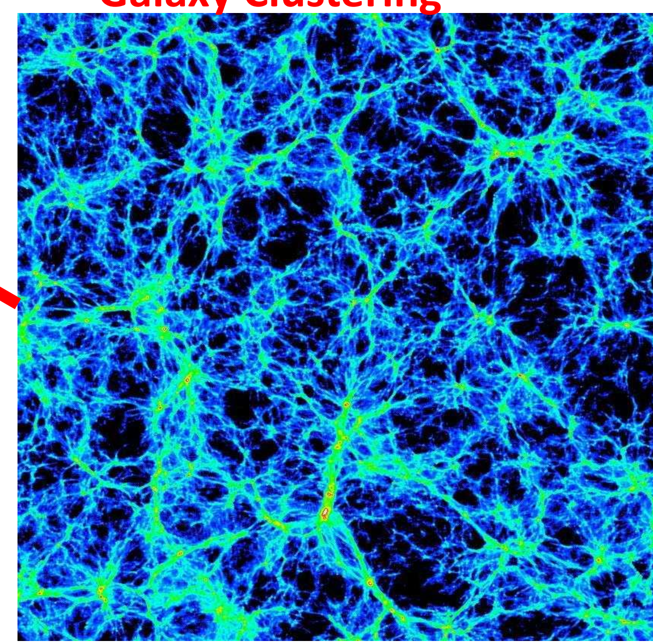

The Euclid sky

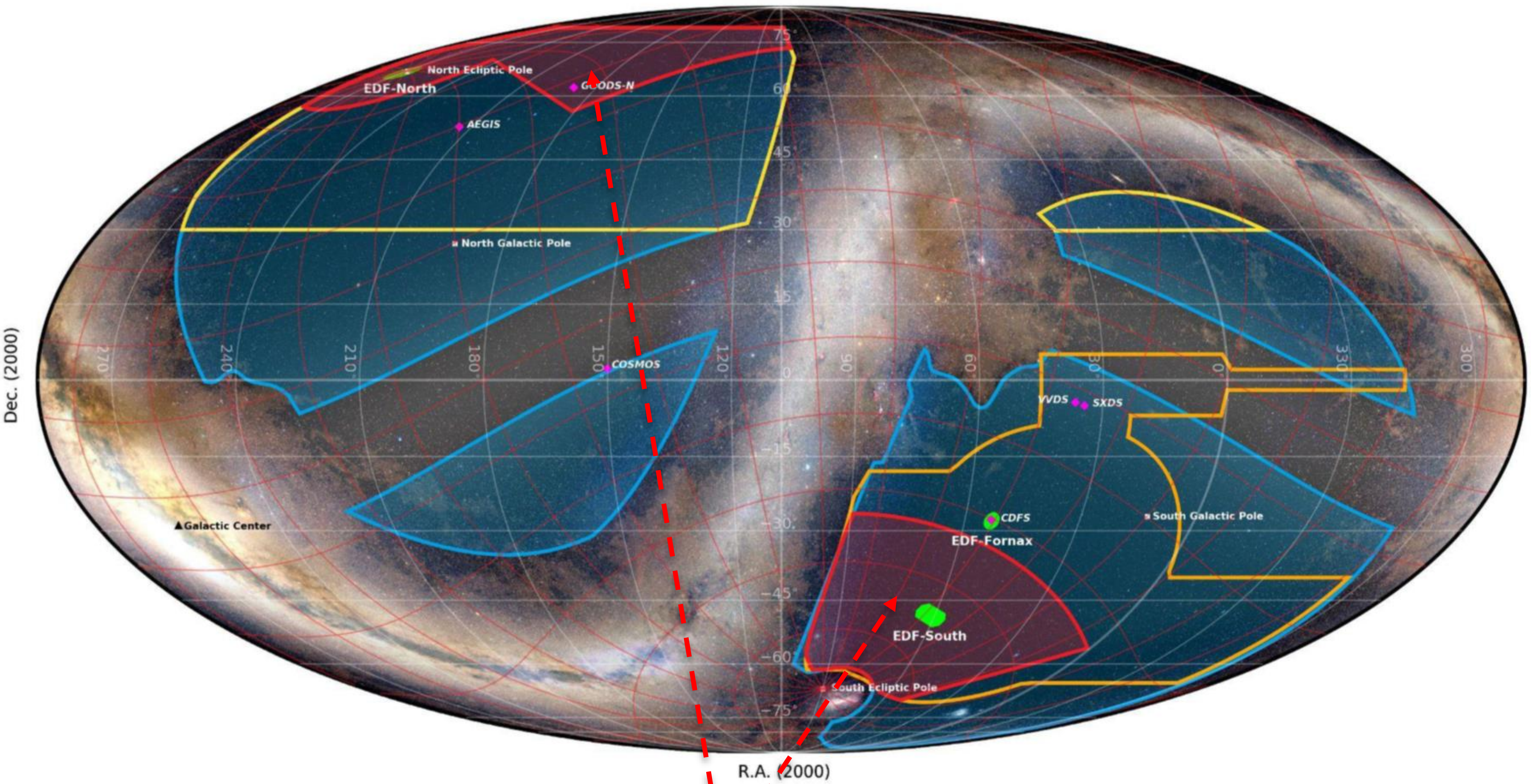

The Euclid Wide Survey DR1 area maximizing the overlap with DES : North = 821 deg^2, South = 1657 deg^2 [Mollweide Celestial]

- Euclid Wide Survey region of interest : 17,354 deg^2
- Euclid DR1 area, 2023 : 2500 deg^2
- DES, griz, 2013−19 : 4500 deg^2 overlap with the region of interest
- Euclid Deep Fields [total 43 deg^2]
- UNIONS [CFIS / JEDIS−g / Pan−STARRS / WISHES], ugriz, 2017−27 : 4800 deg^2

Background image: Euclid Consortium / Planck Collaboration / A. Mellinger

Credits: J.-C. Cuillandre and the ECSURV team

Euclid payload: two instruments for two probes

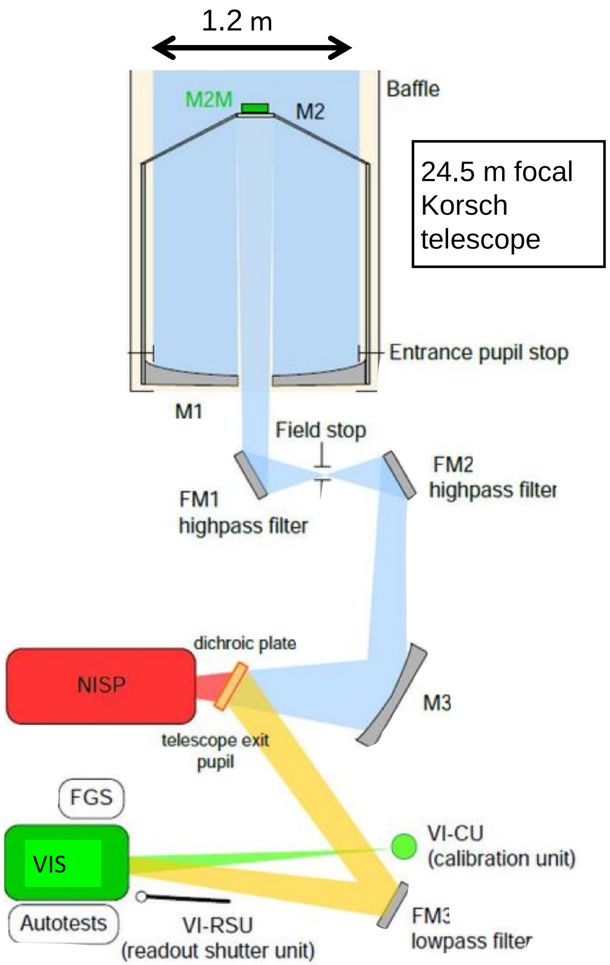

Overview of the PLM sub-systems – Courtesy Airbus Defence and Space.

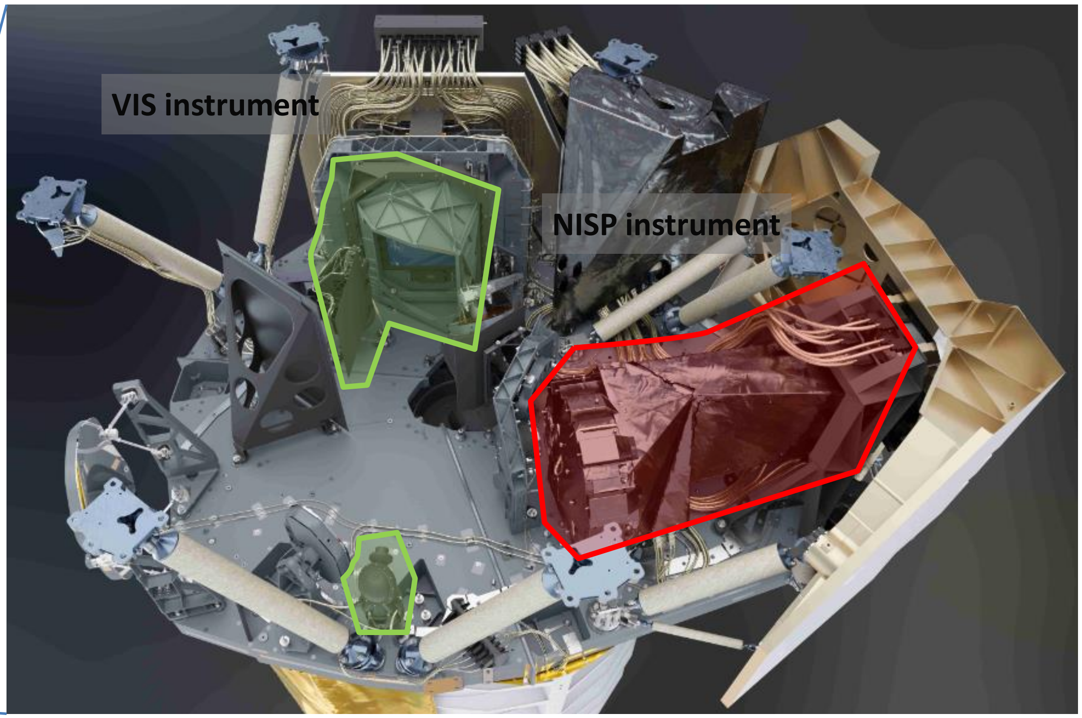

Photo: courtesy ESA/TAS

Euclid: dual wide-field imager

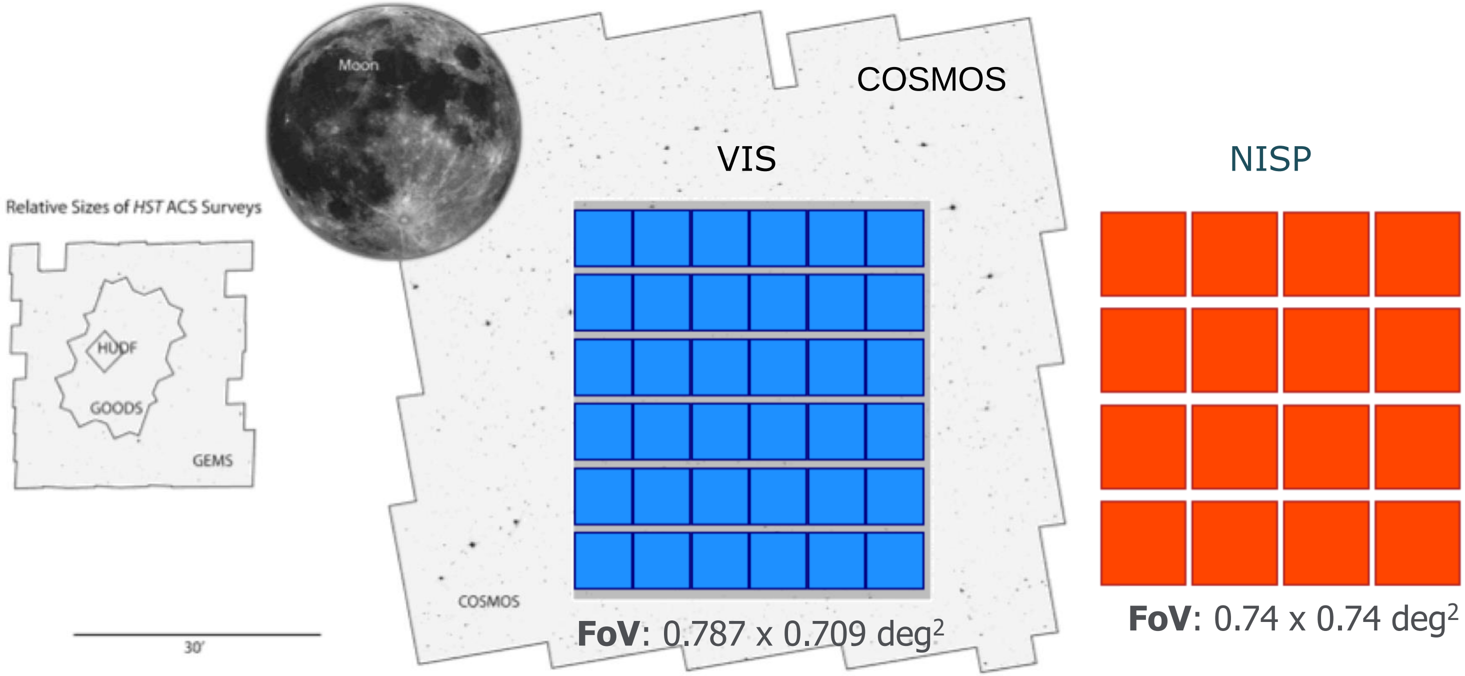

Credit: Space Telescope Science Institute/Nick Scoville (Caltech)

VIS and NISP are both wide field imagers covering about 0.55 deg^2

VIS has 36 CCDs with pixel size 0.1", enabling the weak lensing science.

NISP has 16 detectors with pixel size 0.3".
The spectroscopy resolution will be about 380, which will be well sampled with 13.4"/pixel.

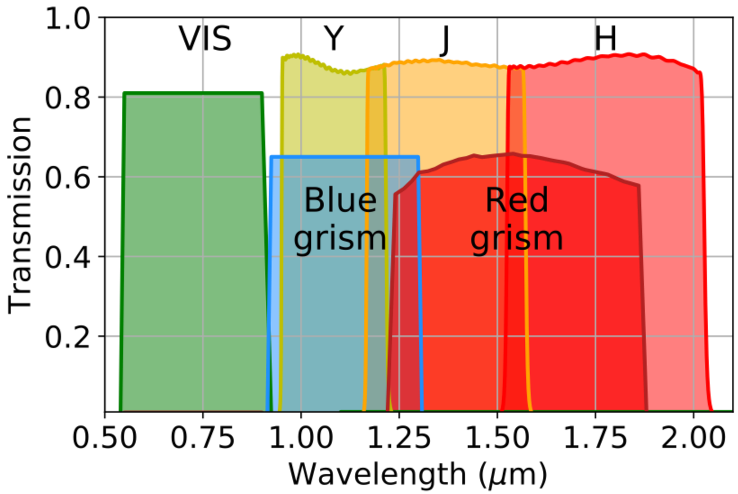

Credits: B. Granett

*Blue grism is exposed on Deep fields only

Euclid Flagship Simulation 1: mock galaxy lightcones

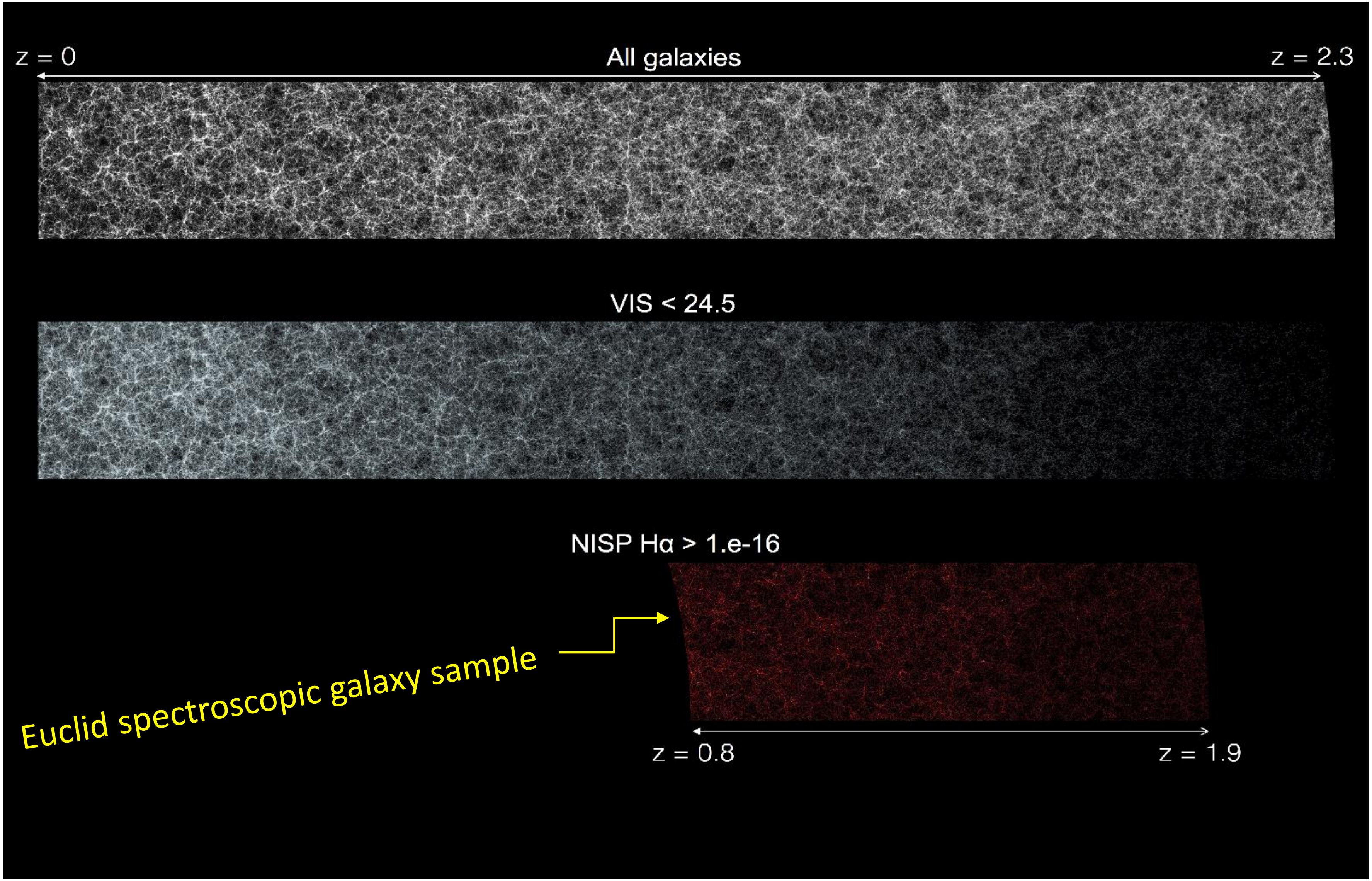

Credits: P. Fosalba

Spectroscopic Galaxy clustering (GCsp): slitless spectroscopy

Credits: B. Granett & e2e group

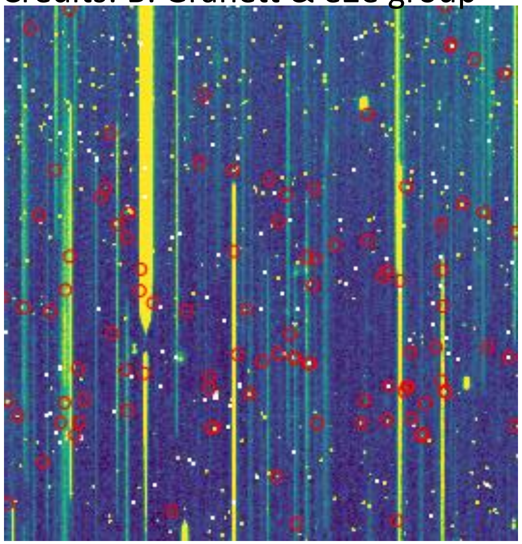

Euclid NISP-S simulated exposure with H_a lines marked

simulated

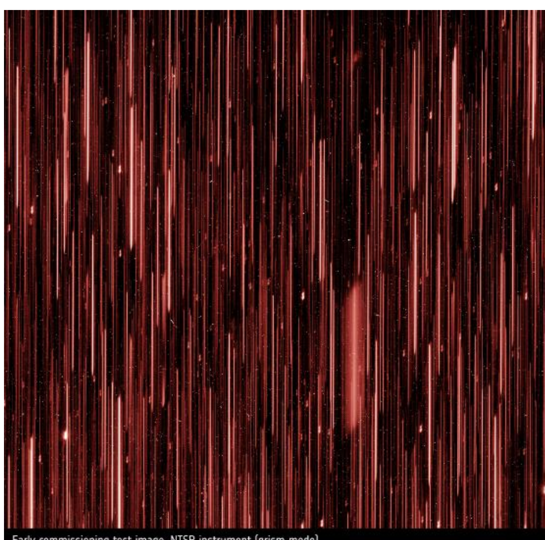

real!

- All photons pass the grism (no slits or fibers)
  - No targeting required
  - Efficiency loss due to higher background
  - Emission line galaxies are main targets
- Euclid is the first large-scale application of this technique
- Slitless spectroscopy is technically simpler, but the resulting selection function is complex: confusion of adjacent spectra makes measuring redshifts more difficult in crowded areas
- Slitless spectroscopy means that almost all spectra are contaminated
- Contamination (or confusion) is biggest source of redshift failures

NISP pointing based on Flagship Sim

Euclid OU-SIM
Field X1:NIP YGH

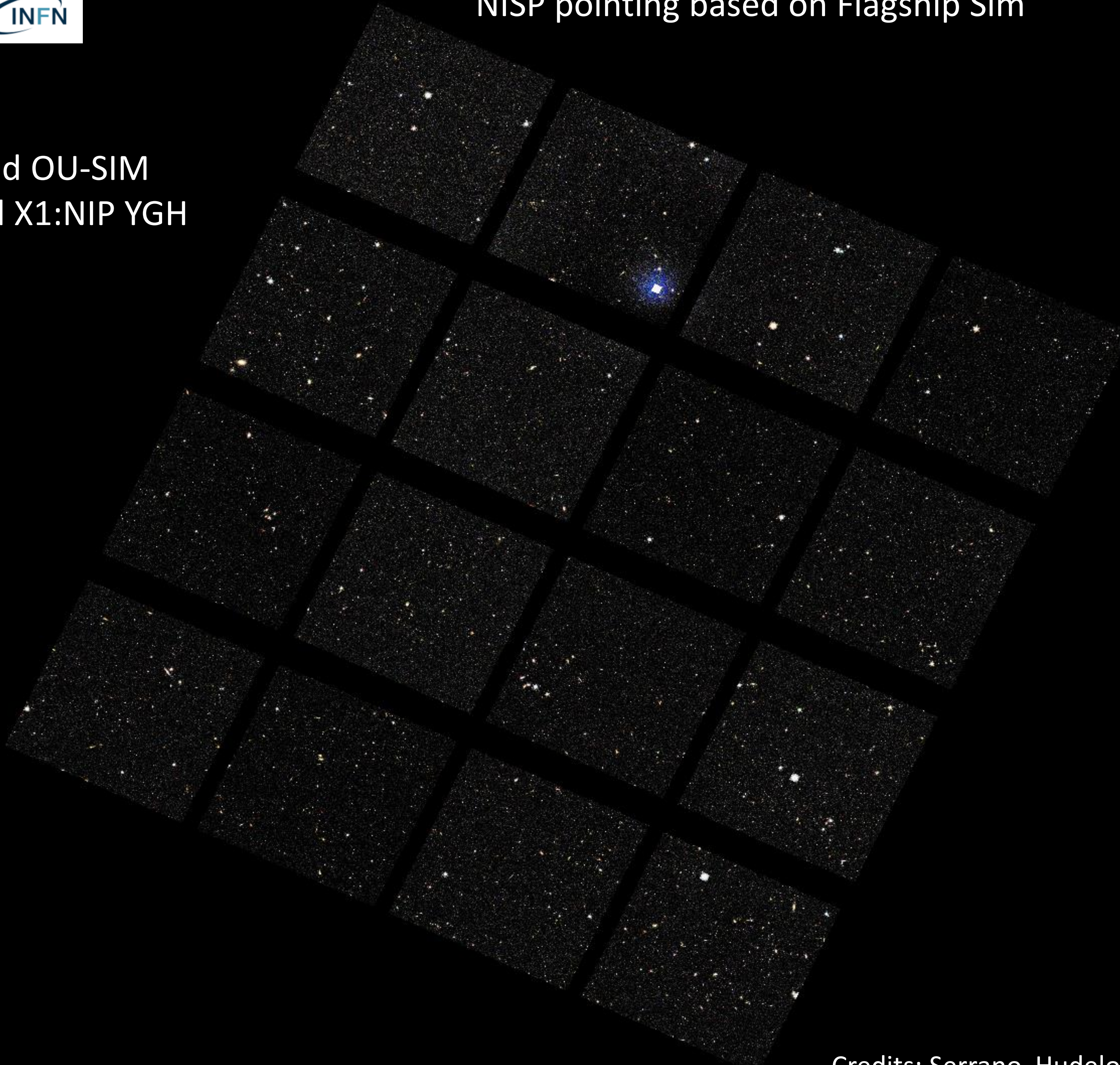

Credits: Serrano, Hudelot & OU-SIM

Corresponding NISP spectroscopic frame

Euclid OU-SIM
Field X1:NIP YGH

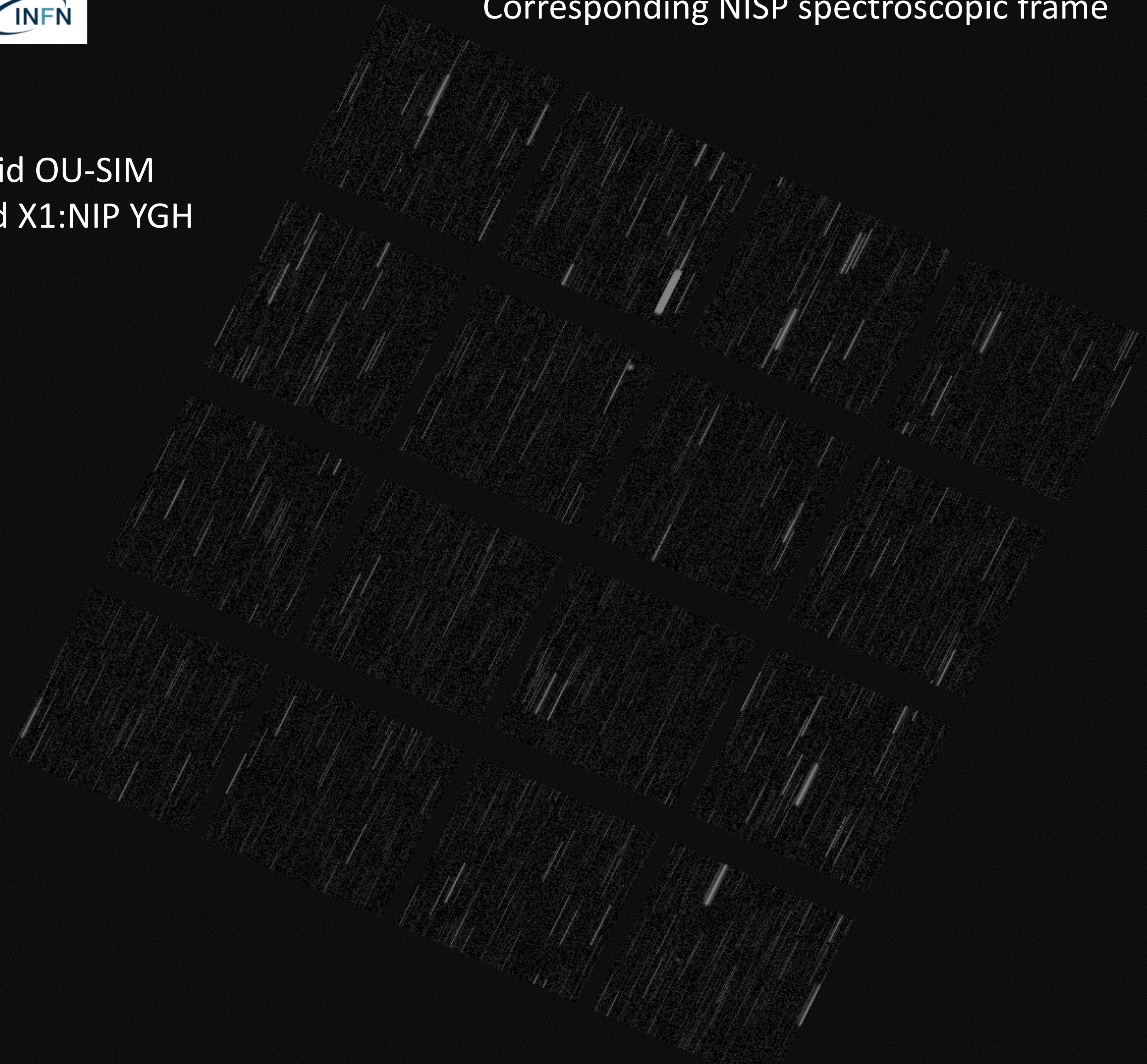

Credits: Serrano, Hudelot & OU-SIM

Slitless spectroscopy: observed galaxy density

- **Completeness:** what fraction of all galaxies expected to a given limit (in Hα flux) will not have a redshift because of confusion?

- **Purity:** what fraction of the measured redshifts is correct (within statistical errors) I.e. how many catastrophic errors do we expect? And which is their redshift distribution?

- **Foregrounds**: zodiacal light and scattered light of Milky Way stars. These will modulate the observed number density

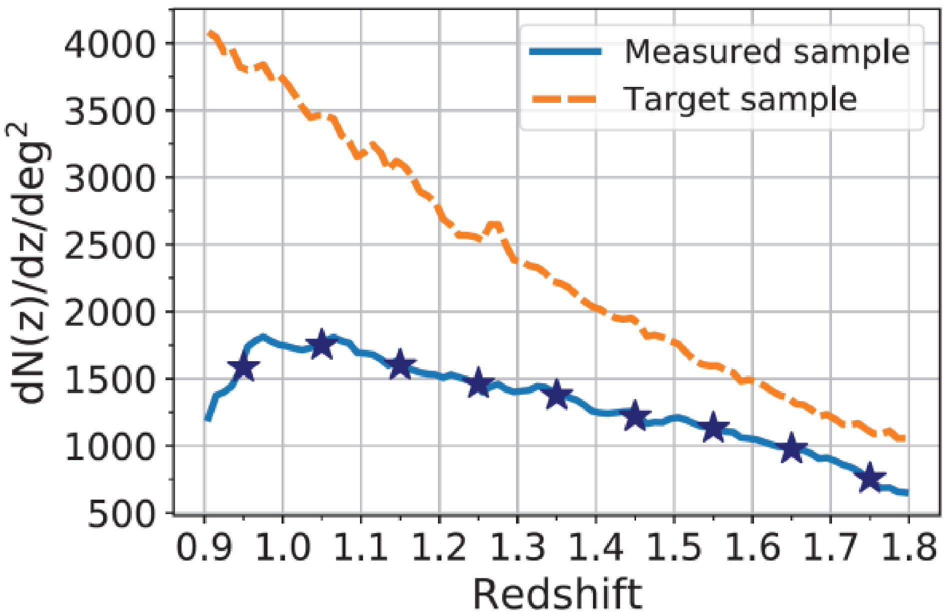

Credits: B. Granett & e2e group

The Euclid spectroscopic survey in context

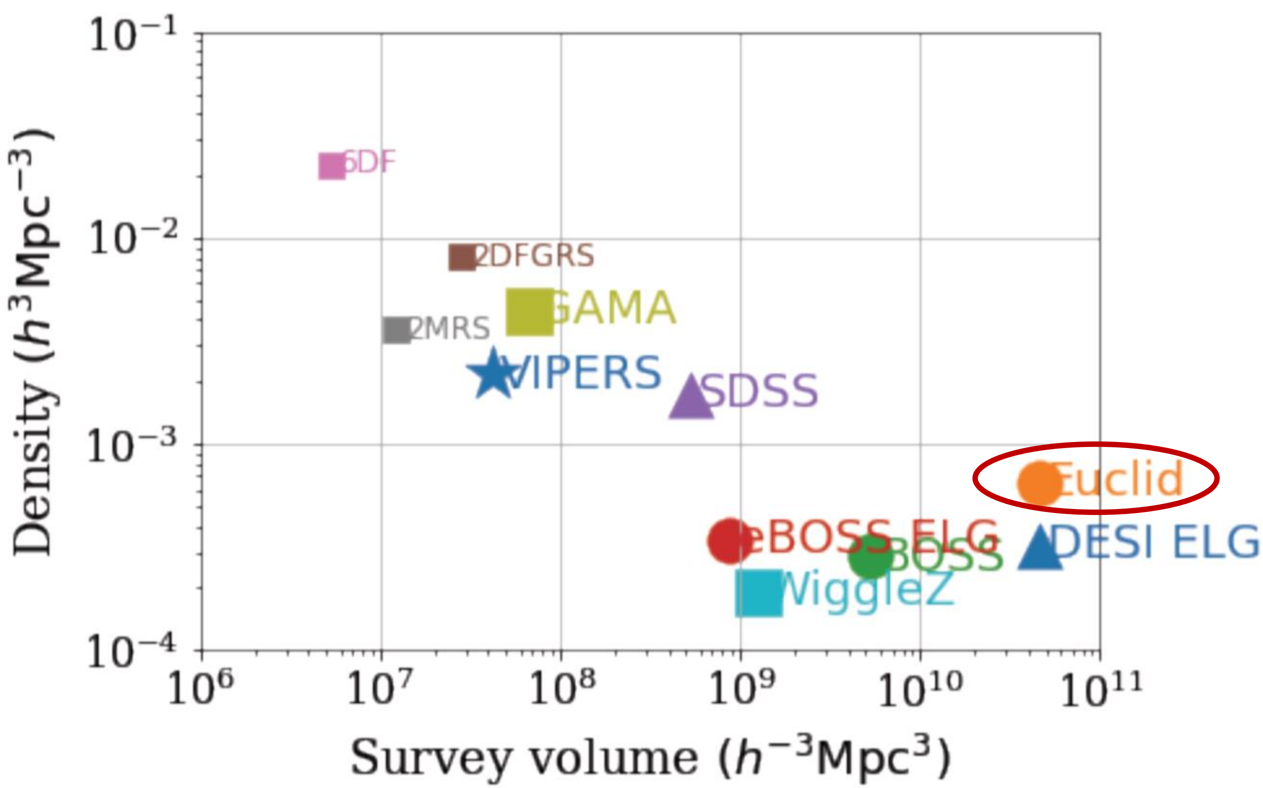

Credits: Ben Granett

GCsp: Baryon Acoustic Oscillations (BAO)

In the early universe prior to recombination, the free electrons couple the baryons to the photons through Compton interactions, so these three species move together as a single fluid.

The primordial cosmological perturbations on small scales excite sound waves in this relativistic plasma, which results in the pressure-induced oscillations and acoustic peak.

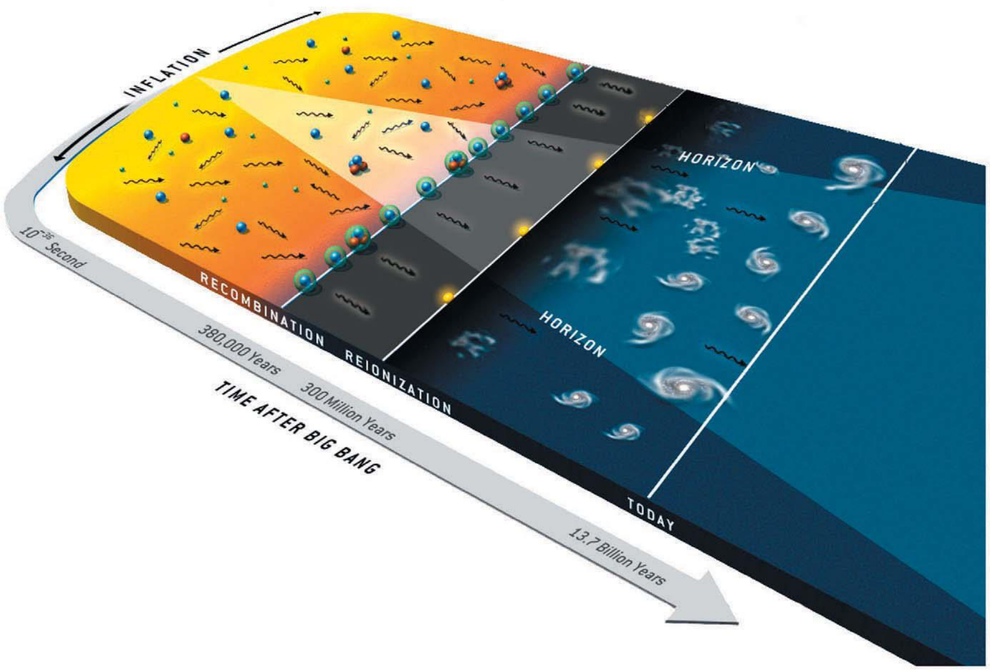

The memory of these baryon acoustic oscillations (BAOs) still remain after the epoch of recombination in the galaxy distribution.

A bit of BAO physics

- Each initial overdensity (in DM & gas) is an overpressure that launches a spherical sound wave.
- This wave travels outwards at 57% of the speed of light.
- Pressure-providing photons decouple at recombination. CMB travels to us from these spheres.
- Sound speed drops rapidly less than the speed of light and wave stalls at a radius of 147.5 Mpc.
- This is seen in CMB as acoustic peaks, and implies a preferred galaxy separation of 147.5 Mpc.

Seo&Eisenstein 2003

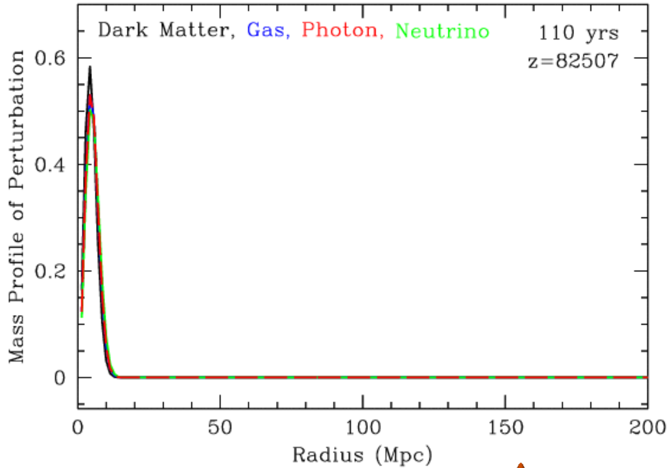

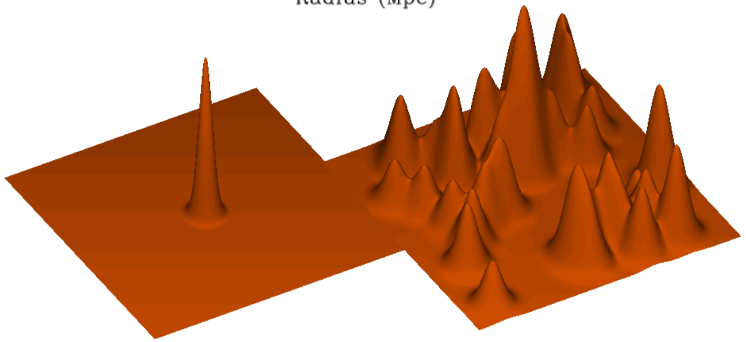

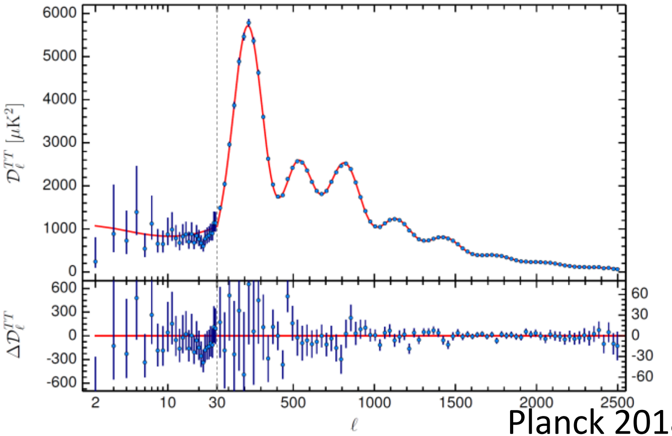

Planck 2018

Euclid GCsp: measuring the background expansion with BAO to 1% precision

Guzzo & GC-SWG (2015)

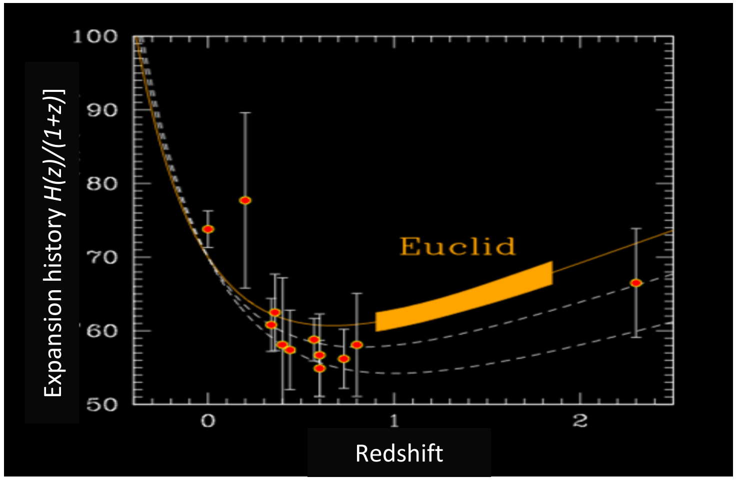

- **BAO** as a *standard ruler*

- Sensitive to the expansion history ***H(z)*** and angular diameter distance relation ***D_A(z)***

$$r_d = \int_{z_d}^{\infty} \frac{c_s(z)}{H(z)} dz = 147.49 \pm 0.59 \ \mathrm{Mpc}$$

need of precise redshifts

$$r_{\parallel} = \frac{c\Delta z}{H(z)}$$

$$r_{\perp} = (1+z) D_A(z) \Delta\theta$$

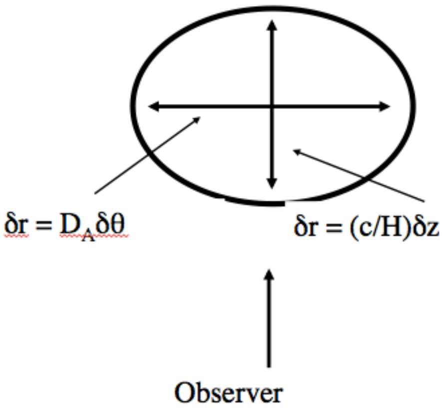

$$D_A(z) = \frac{c}{1+z} \int_0^z \frac{dz}{H(z)} \qquad D_M(z) = (1+z) D_A(z)$$

$$D_H(z) = c/H(z)$$

$$H(z) = h\sqrt{\Omega_m (1+z)^3 + \Omega_X \exp\left[3 \int_0^z \frac{1+w(z)}{1+z} dz\right]}$$

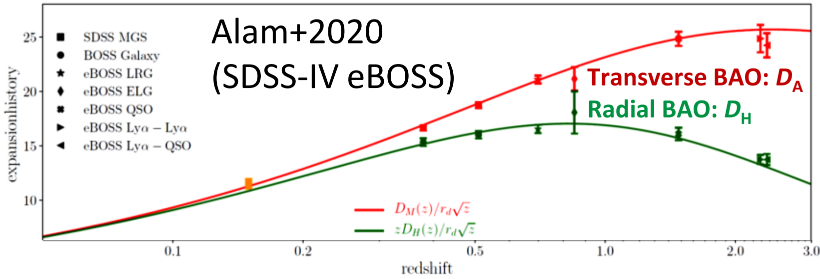

- Test "beyond Λ" scenario, i.e. an evolving equation of state

Acoustic Oscillations in the Early Universe and Today

Due to the significant fraction of baryons in the universe, BAOs are imprinted onto the late time power spectrum of the non-relativistic matter.

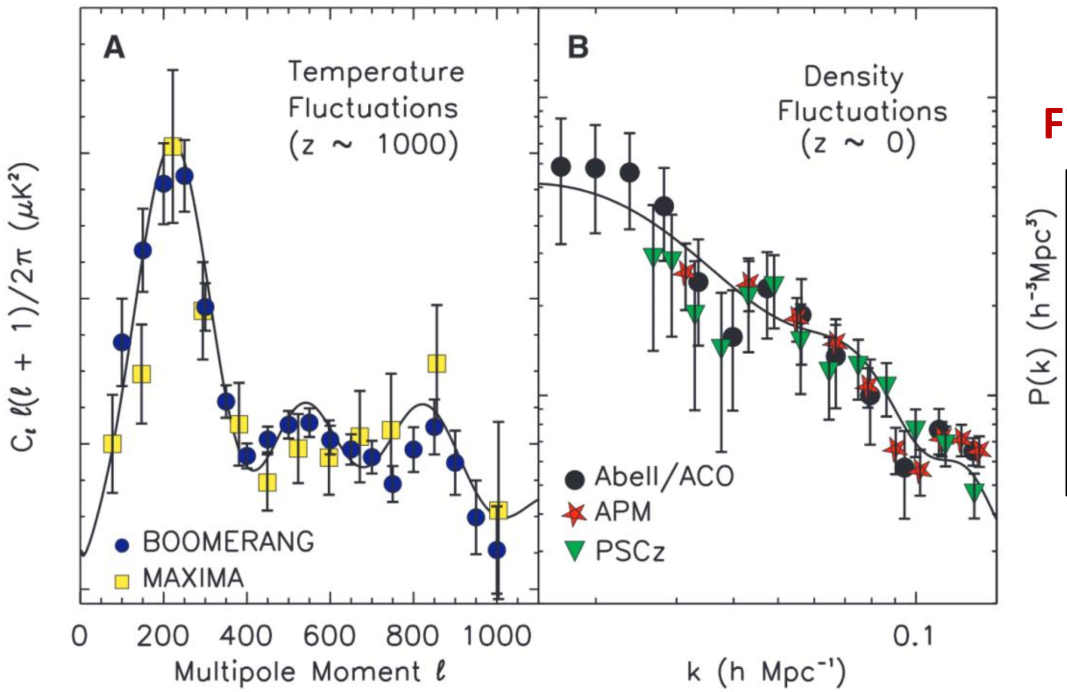

Fig. 1. We plot the CMB data from the MAXIMA and BOOMERANG experiments (**A**) alongside the matter-density data (**B**). The solid line is the best fit model ($\Omega_{\text{matter}} = 0.24$, $\Omega_{\text{baryons}} = 0.06$, and $n_s = 1.08$ with $H_0 = 69$) using the matter-density data alone. The amplitudes in both plots remain a free parameter. The solid line in (A) is not a fit to the CMB data (although the χ^2 is 34 for 32 data points). It is the resultant cosmological model using the best fit parameters from (B) and $\Omega_{\text{vacuum}} =$ 0.8, consistent with the Type Ia supernovae results (*18*).

First detections of BAO in CMB and LSS

During its first $\simeq$100,000 years, the universe was a fully ionized plasma with a tight coupling by Thompson scattering between the photons and matter. The trade-off between gravitational collapse and photon pressure causes acoustic oscillations in this primordial fluid. These oscillations will leave predictable imprints in the spectra of the cosmic microwave background and the present-day matter-density distribution. Recently, the BOOMERANG and MAXIMA teams announced the detection of these acoustic oscillations in the cosmic microwave background (observed at redshift $\simeq$ 1000). Here, we compare these CMB detections with the corresponding acoustic oscillations in the matter-density power spectrum (observed at redshift $\simeq$ 0.1). These consistent results, from two different cosmological epochs, provide further support for our standard Hot Big Bang model of the universe.

MILLER, NICHOL, BATUSKI, *SCIENCE,* 24 May 2001, Vol 292, Issue 5525, pp. 2302-2303, DOI: 10.1126/science.1060440

BAO in the galaxy power spectrum and correlation function

Oscillation in the power spectrum (Hankel transfor of \xi)

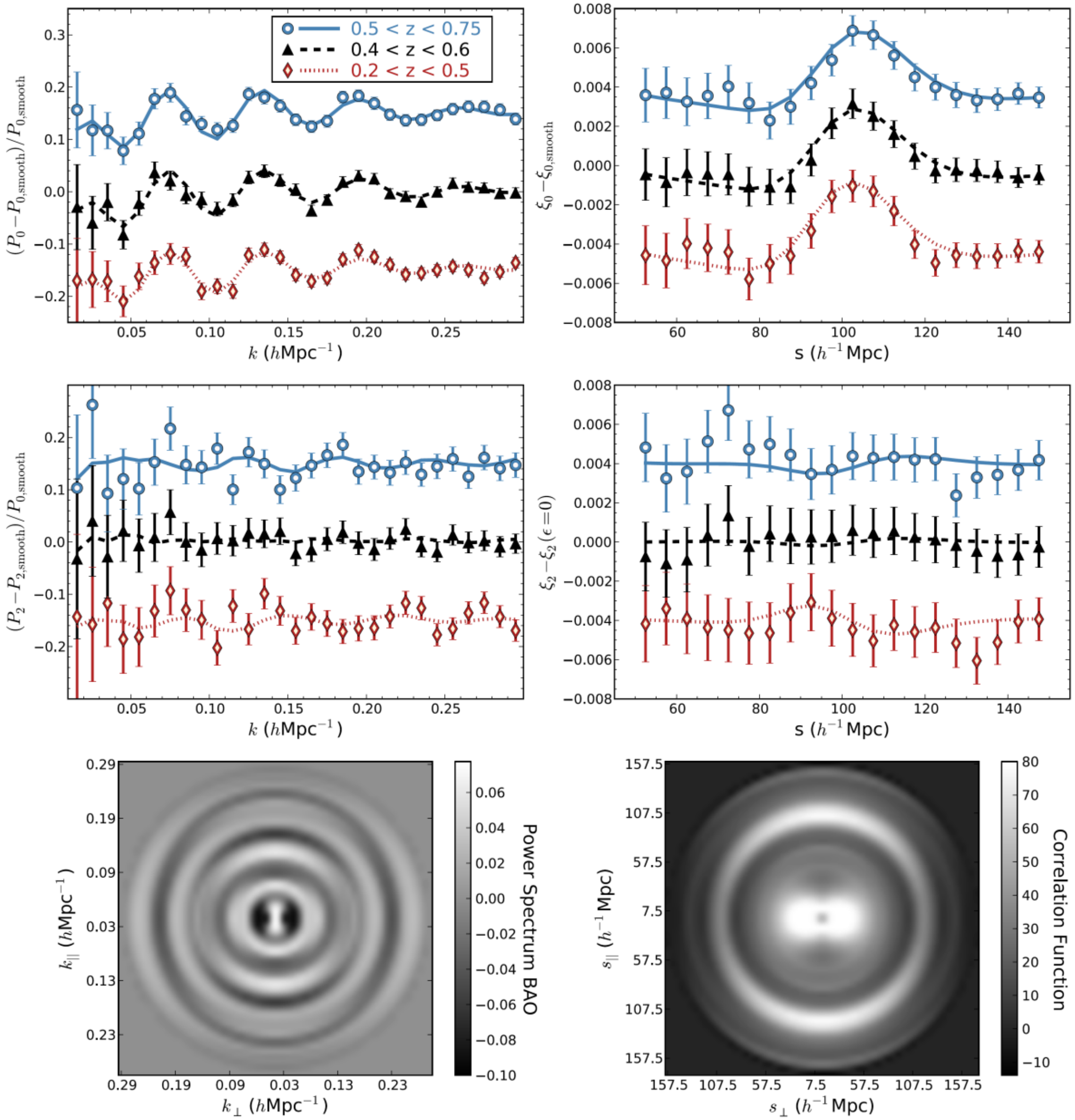

Peak at 150 Mpc in the correlation function

Alam+16 (SDSSIII BOSS)

Current BAO, SN, and CMB constraining power as a function of redshift

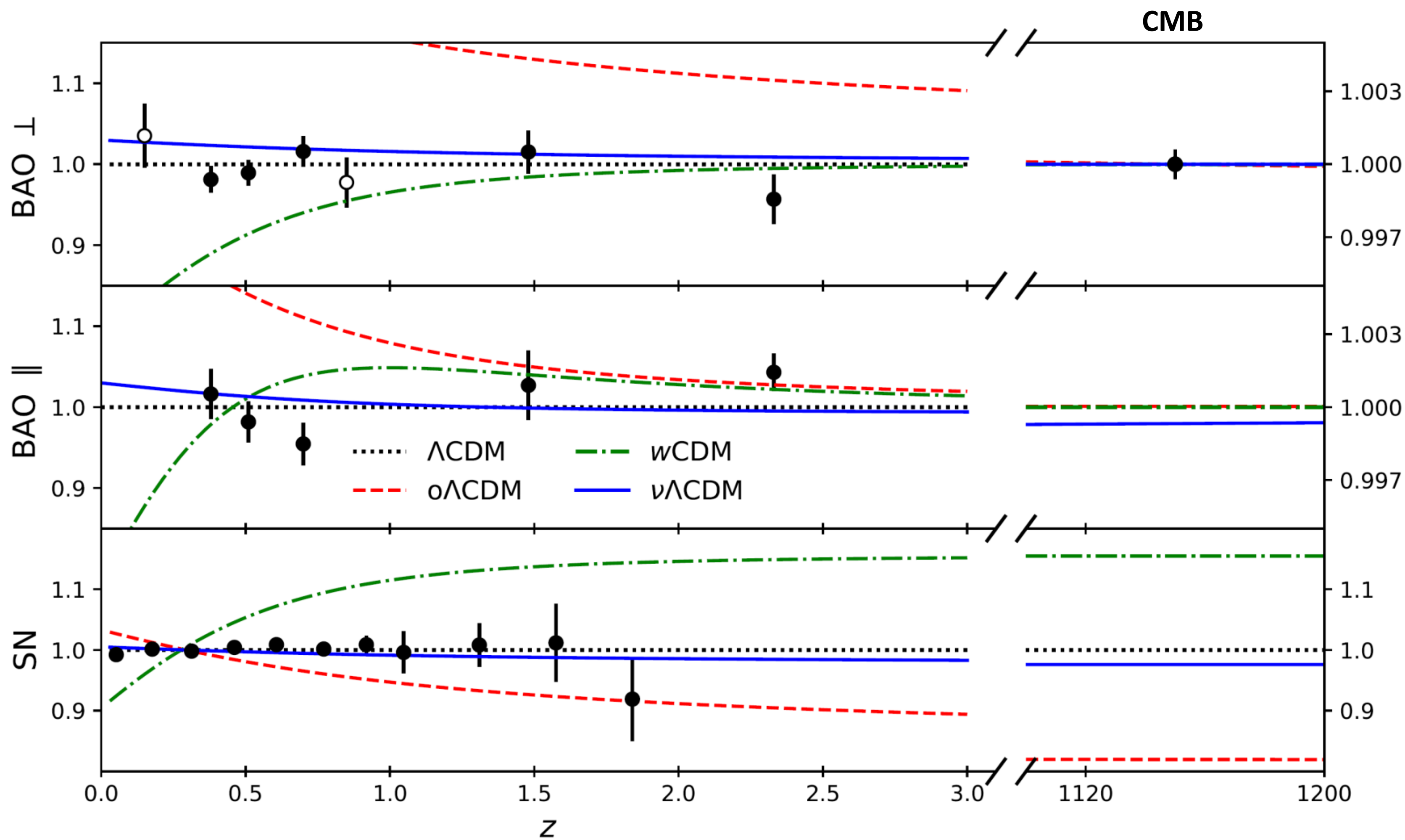

Alam+2020 (SDSS-IV)

GCsp: Redshift Space Distortions (RSD)

Growth rate produces peculiar velocities, which combine with the cosmological Hubble flow in measured redshifts

$r \equiv H_0 d$ $\quad$ $s = r + v$ $\quad$ $s \equiv cz$

observed distance

The galaxy correlation function becomes *anisotropic*

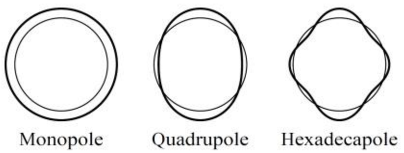

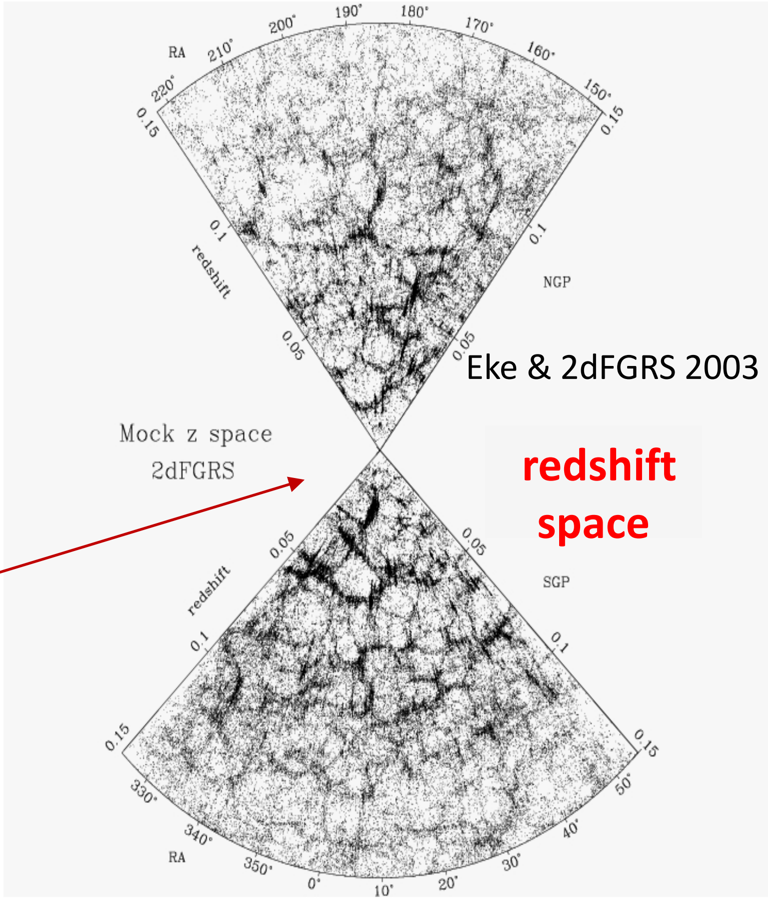

RSDs: 1) the **Kaiser effect** which *flattens* the galaxy distribution and is caused by coherent motions of galaxies falling inwards towards the cluster centre. The Kaiser effect is smaller and occurs on larger scales than FoGs.

2) the **FoG (fingers-of-God) nonlinear effect** which *elongates* the galaxy distribution along the line-of-sight, caused by the Doppler shift due to random galaxy peculiar velocities within the cluster

A bit of RSD physics

dot <- -> galaxy

arrow <- -> peculiar velocity

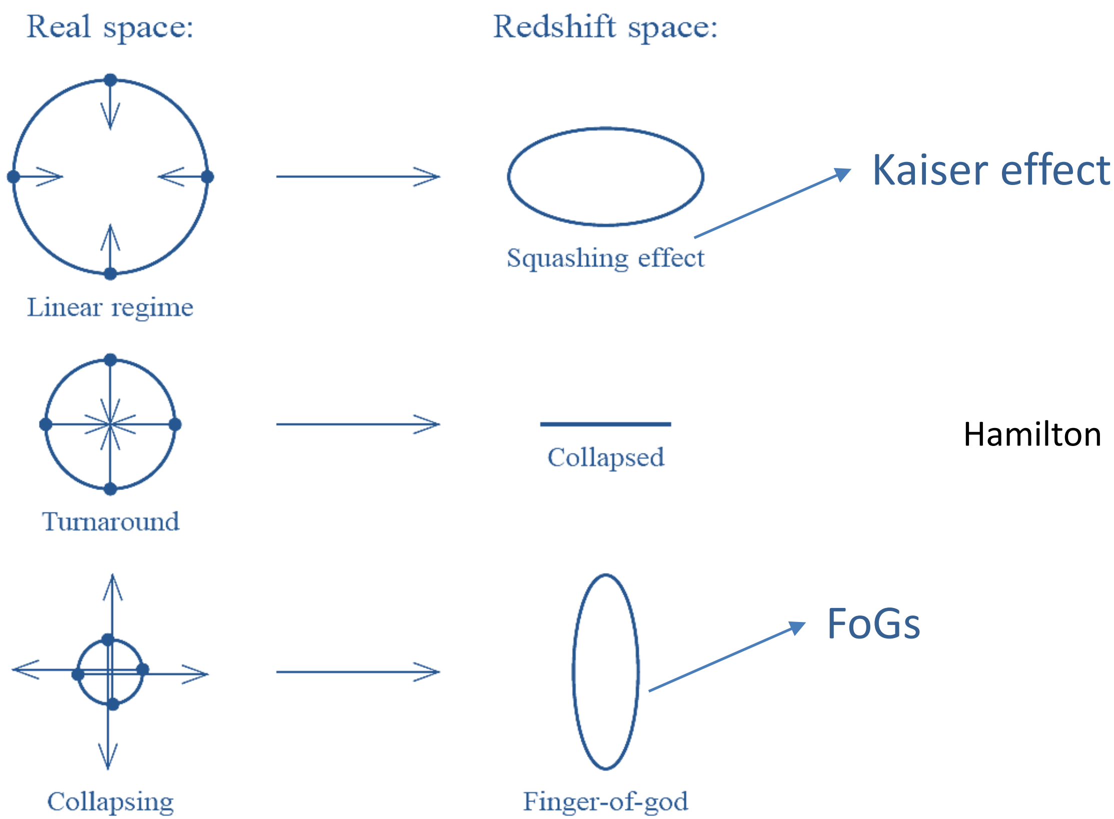

Hamilton 1997

a) At large scales, the peculiar velocity of an infalling shell is small compared to its radius, and the shell appears squashed.
b) At smaller scales, the shell radius is smaller and its peculiar infall velocity tends to be larger. The shell that is just at turnaround, its peculiar velocity just cancelling the general Hubble expansion, appears collapsed to a single velocity in redshift space.
c) At yet smaller (nonliner) scales, shells that are collapsing in proper coordinates appear inside out in redshift space. The combination of collapsing shells with previously collapsed, virialized shells, gives rise to fingers-of-god.

The galaxy correlation function $\xi(r_p,\pi)$ in RS

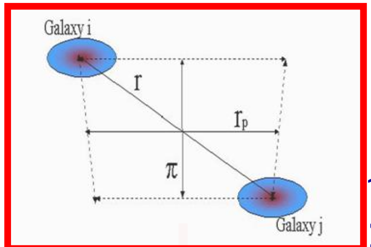

Line of sight to observer

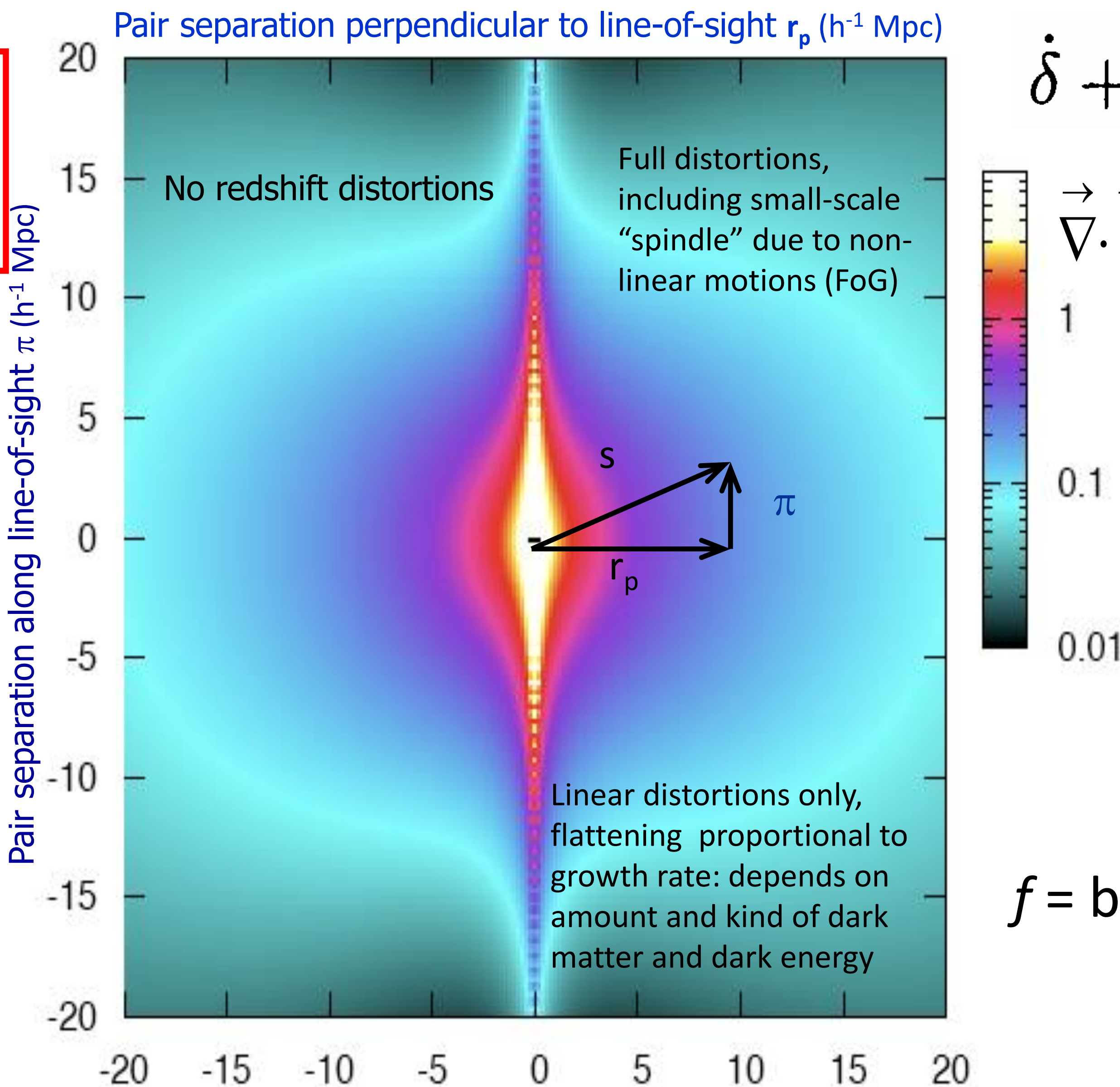

$$\dot{\delta} + ikv = 0$$

$$\vec{\nabla} \cdot \vec{v} = -a\delta Hf$$

$$f = b_L \beta$$

Credits: Gigi Guzzo

GCsp: measuring the structure growth with RSD to 1% precision

Guzzo & GC-SWG (2015)

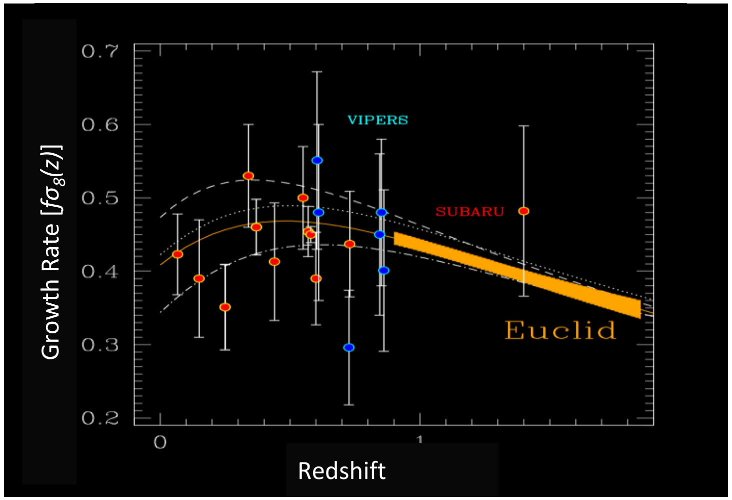

- **RSDs probe the growth rate of structure**

$$z_{\rm obs} = z_{\rm c} + \frac{v_\parallel}{c}(1+z_{\rm c})$$

$$\frac{\xi(s)}{\xi(r)} \overset{\text{linear limit}}{=} 1 + \frac{2\beta}{3} + \frac{\beta^2}{5}$$

$$\beta \;=\; f(z)/b(z) \;\simeq\; \Omega_{\rm m}(z)^{\gamma}/b(z)$$

$$\boxed{P_{\rm zs}(k,\mu,z) = \left[\frac{1}{1+(f(z)k\mu\,\sigma_{\rm p}(z))^2}\right]\left(b(z)\sigma_8(z)+f(z)\sigma_8(z)\mu^2\right)^2\frac{P_{\rm dw}(k,z)}{\sigma_8^2(z)}}$$

$$P_{\rm dw}(k,z) = [P_{\rm m}(k,z) - P_{\rm nw}(k,z)]\,{\rm e}^{-g_\mu k^2} + P_{\rm nw}(k,z)$$

BAO only x damping + Broadband

$$\boxed{g_\mu(k,\mu,z) = \sigma_{\rm v}^2(z)\left[1-\mu^2+\mu^2\left(1+f(z)\right)^2\right]}$$

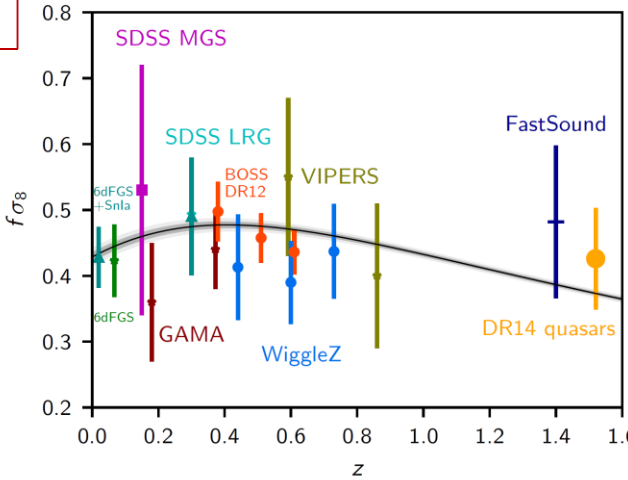

- **Test “beyond Einstein” scenario as alternative to GR**

Planck-I 2018

RSD in the galaxy power spectrum and correlation function

$\xi(r_p,\pi)$

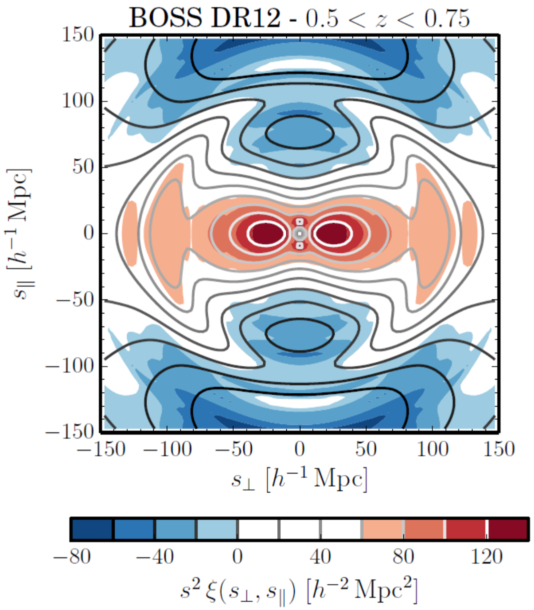

$P(k,\mu)$

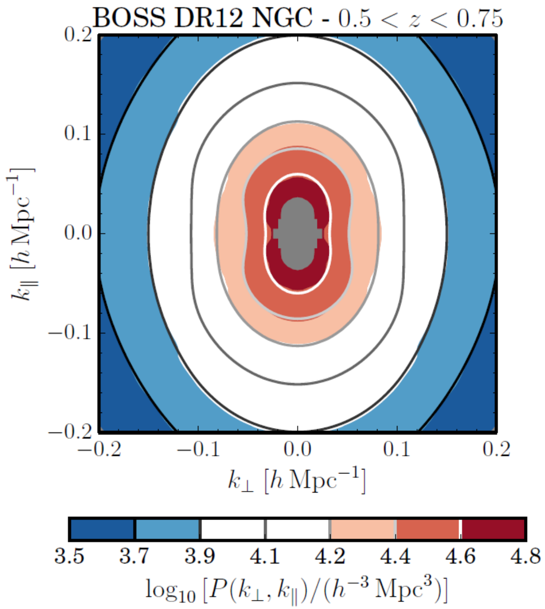

Alam et al 2016 (SSDIII-BOSS)

The measured pre-reconstruction correlation function (left) and power spectrum (middle) in the directions perpendicular and parallel to the line of sight, shown for the NGC only in the redshift range 0.50 < z < 0.75. In each panel, the color scale shows the data and the contours show the prediction of the best-fit model. The anisotropy of the contours seen in both plots reflects a combination of RSD and the AP effect, and holds most of the information used to separately constrain DM(z)/rd, H(z)rd, and fs8. The BAO ring can be seen in two dimensions on the correlation function plot.

Current growth rate measurements as a function of redshift from eBOSS

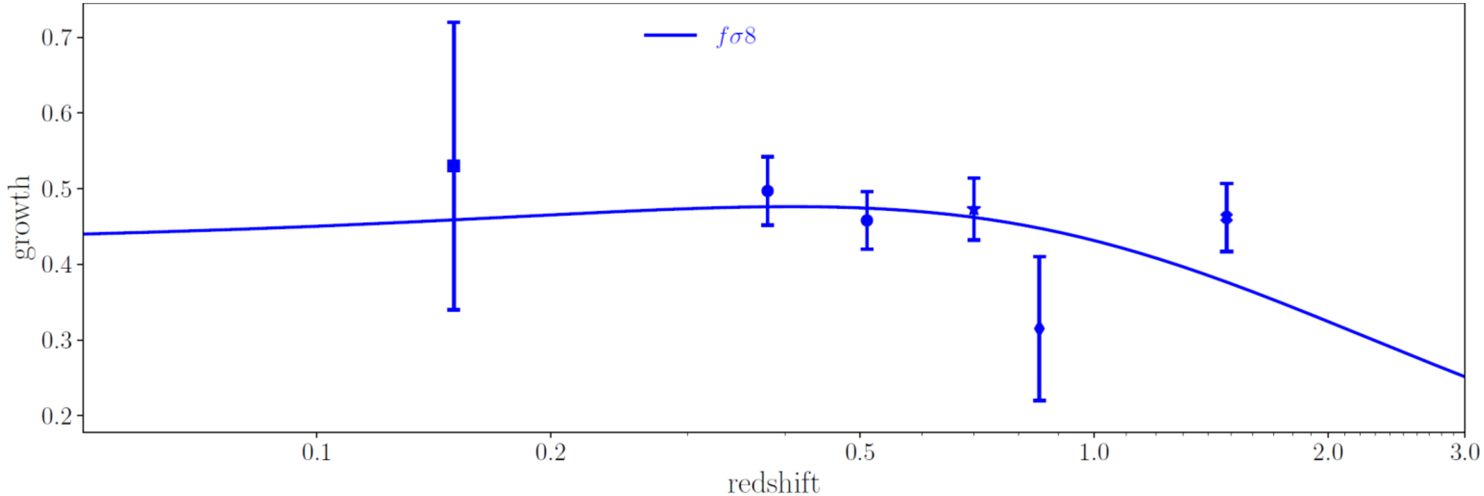

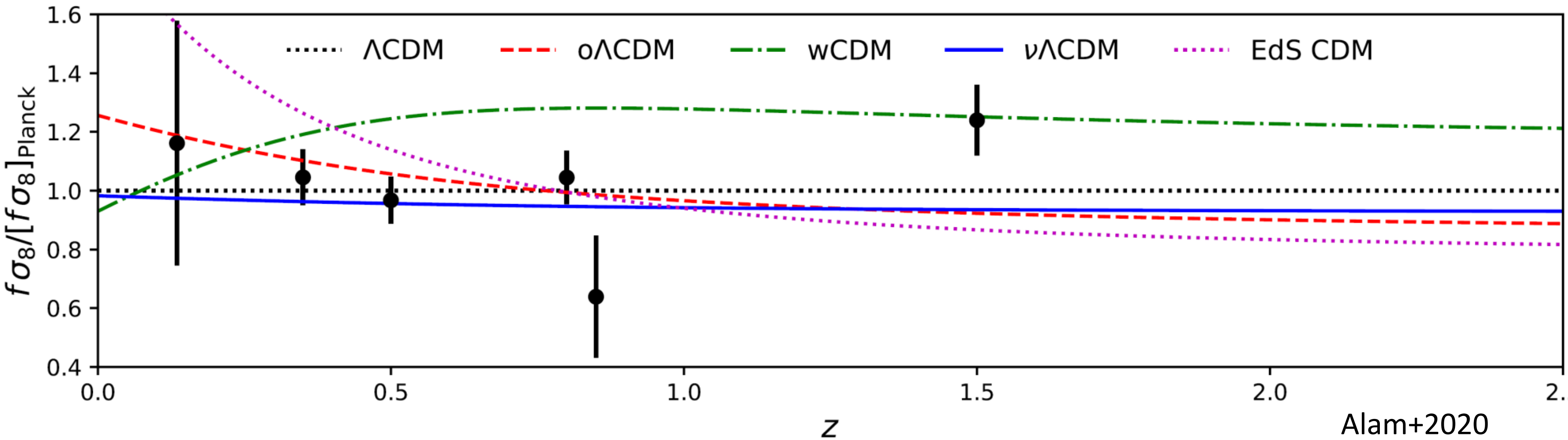

Alam+2020
(SDSS-IV eBOSS)

Clustering in real and redshift space

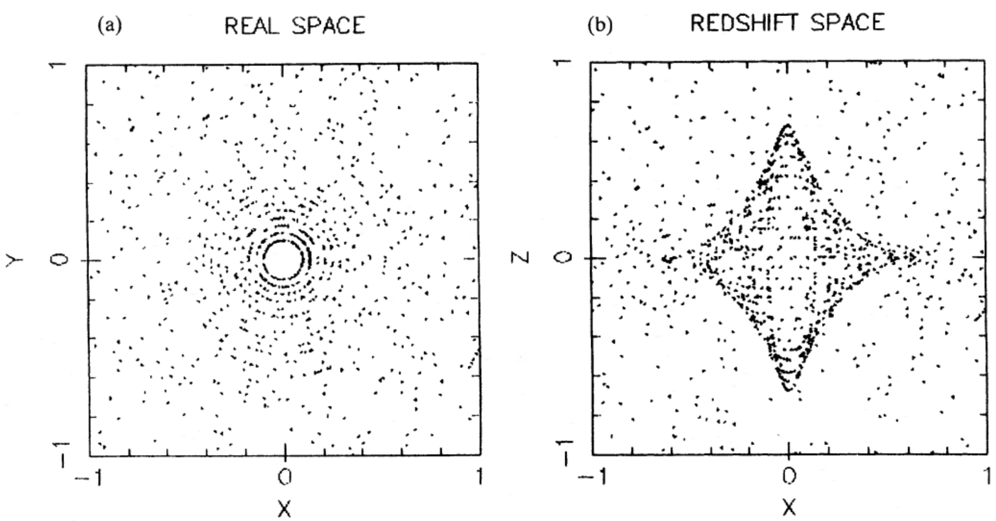

Figure 5. Spherical cluster with power law density profile in *r*-space (a) and as it appears in redshift space (b). The points shown are those which lie in a thin equatorial slice through the cluster centre. Points in the central virialized portion have been omitted. Innermost points are falling into the cluster for the first time. The sampling density and separation between shells are such that individual shells can still be seen in *s*-space (*z*-coordinate is the redshift direction). The density contrast profile is $\Delta(r)=(r/1.4)^{-1.75}$. A caustic surface has resulted in *s*-space which, in three dimensions, has the form of two trumpet horns glued face to face. The caustic surface extends to the turnaround radius which lies at roughly twice the central 1D velocity dispersion, or about $20\,h^{-1}$ Mpc for a cluster like Coma.

Summary. Peculiar velocities distort the clustering pattern in redshift space on all scales. Four consequences of this are:

(i) The acceleration vector derived by summing the inverse squared redshifts of galaxies differs significantly from the true acceleration even in linear theory. Estimates of Ω obtained in this manner are only reliable for small Ω.

(ii) The power spectrum of large-scale clustering has a quadrupole anisotropy, providing a way to estimate Ω. We calculated, for various assumed power spectra, the line-of-sight correlation function in redshift space, ξ_v. We find that ξ_v may display a strong anticorrelation feature that has no counterpart in real space.

(iii) The density contrast of the local supercluster will appear enhanced in redshift space. Using a simple infall model (with Ω=1), we simulate the Shapley–Ames catalogue. For an infall velocity around $350\,\mathrm{km\,s^{-1}}$, the apparent density is similar to that observed, so the data do not require $\Omega \ll 1$, or biasing on large scales.

(iv) Turnaround is estimated to occur at a radius $\simeq 1500\,\mathrm{km\,s^{-1}}$ from a rich cluster, resulting in large transverse features of this scale. Since the velocity field is apparently very coherent, high density caustic surfaces must result. Guided by the appearance of the spherical model, we argue that the shell-like structures seen in some recent redshift surveys are most naturally interpreted as these caustics, rather than as the result of energetic explosions. The model also shows the apparent falling velocity dispersion with radius that is often seen in rich clusters, and suggests that the interpretation of this in terms of equilibrium models is inappropriate.

First mathematical description of RSD

Nick Kaiser, *Monthly Notices of the Royal Astronomical Society*, Volume 227, Issue 1, July 1987, Pages 1-21
https://doi.org/10.1093/mnras/227.1.1

Euclid Top Level Science Requirements

Sector	Euclid Targets
Dark Energy	· Measure the cosmic expansion history to better than 10% in redshift bins $0.9 < z < 1.8$. · Look for deviations from $w = -1$, indicating dynamical Dark energy. · Euclid ***primary probes*** to give **FoM$_{DE}$ $\geq$ 400** (1-sigma errors on w_p & w_a of 0.02 and 0.1 respectively)
Test Gravity	· Measure the growth index, γ, with a precision better than 0.02 · Measure the growth rate to better than 0.02 in redshift bins between $0.9< z < 1.8$ · Separately constrain the two relativistic potentials. ψ and ϕ · Test the cosmological principle
Dark Matter	· Detect Dark matter halos on a mass scale between 10^8 and 10^{15} M_{Sun} · Measure the Dark matter mass profiles on cluster and galactic scales · Measure the sum of neutrino masses with an accuracy of 0.03 eV
Initial Conditions	· Measure the matter power spectrum on a large range of scales in order to extract values for the parameters σ_8 and n to a 1-sigma accuracy of 0.01. · For extended models, improve constraints on spectral indices n and α wrt to Planck alone by a factor 2. · Measure a non-Gaussianity parameter : f_{NL} for local-type models with an error < +/-2.

- *DE equation of state: $P/\rho = w$ with $w(a) = w_p + w_a(a_p-a)$*
- *Growth rate of structure formation: $f \sim \Omega^\gamma$;*
- *FoM=1/(Δw_a x Δw_p) > 400→ ~2% precision on w_p*

Euclid Redbook

The GC_{sp}+3x2pt Euclid primary probes

(GC_{sp}+WL+GC_{ph}+WLxGC_{ph})

Modelling used for Fisher forecasts (IST:F) arXiv:1910.09273

GCsp

$$P_{\rm obs}(k_{\rm ref},\mu_{\rm ref};z) = \frac{1}{q_\perp^2 q_\parallel}\left\{\frac{\left[b\sigma_8(z)+f\sigma_8(z)\mu^2\right]^2}{1+\left[f(z)k\mu\sigma_{\rm p}(z)\right]^2}\right\}\frac{P_{\rm dw}(k,\mu;z)}{\sigma_8^2(z)}F_z(k,\mu;z)+P_{\rm s}(z)$$

$$C_{ij}^{\rm LL}(\ell) = \int_{z_{\rm min}}^{z_{\rm max}} \frac{dz}{H(z)r^2(z)}\mathcal{W}_i^{\rm L}(z)\mathcal{W}_j^{\rm L}(z)P_{\delta\delta}\left(\frac{\ell+1/2}{r(z)},z\right)$$

$$C_{ij}^{\rm GL}(\ell) = \int \frac{dz}{H(z)r^2(z)}\mathcal{W}_i^{\rm G}(z)\,\mathcal{W}_j^{\rm L}(z)P_{\delta\delta}\left(\frac{\ell+1/2}{r(z)},z\right)$$

No magnification bias

$$C_{ij}^{\rm GG}(\ell) = \int \frac{dz}{H(z)r^2(z)}\mathcal{W}_i^{\rm G}(z)\,\mathcal{W}_j^{\rm G}(z)P_{\delta\delta}\left(\frac{\ell+1/2}{r(z)},z\right)$$

$$\mathcal{W}_i^{\rm L} = W_i^\gamma(z) - \frac{\mathcal{A}_{\rm IA}\mathcal{C}_{\rm IA}\Omega_{\rm m}\mathcal{F}_{\rm IA}(z)}{D(z)}W_i^{\rm IA}(z)$$

3x2pt=WL+GC_{ph}+WLxGC_{ph}

Weight functions for GC_{ph}, GC_{sp} & WL

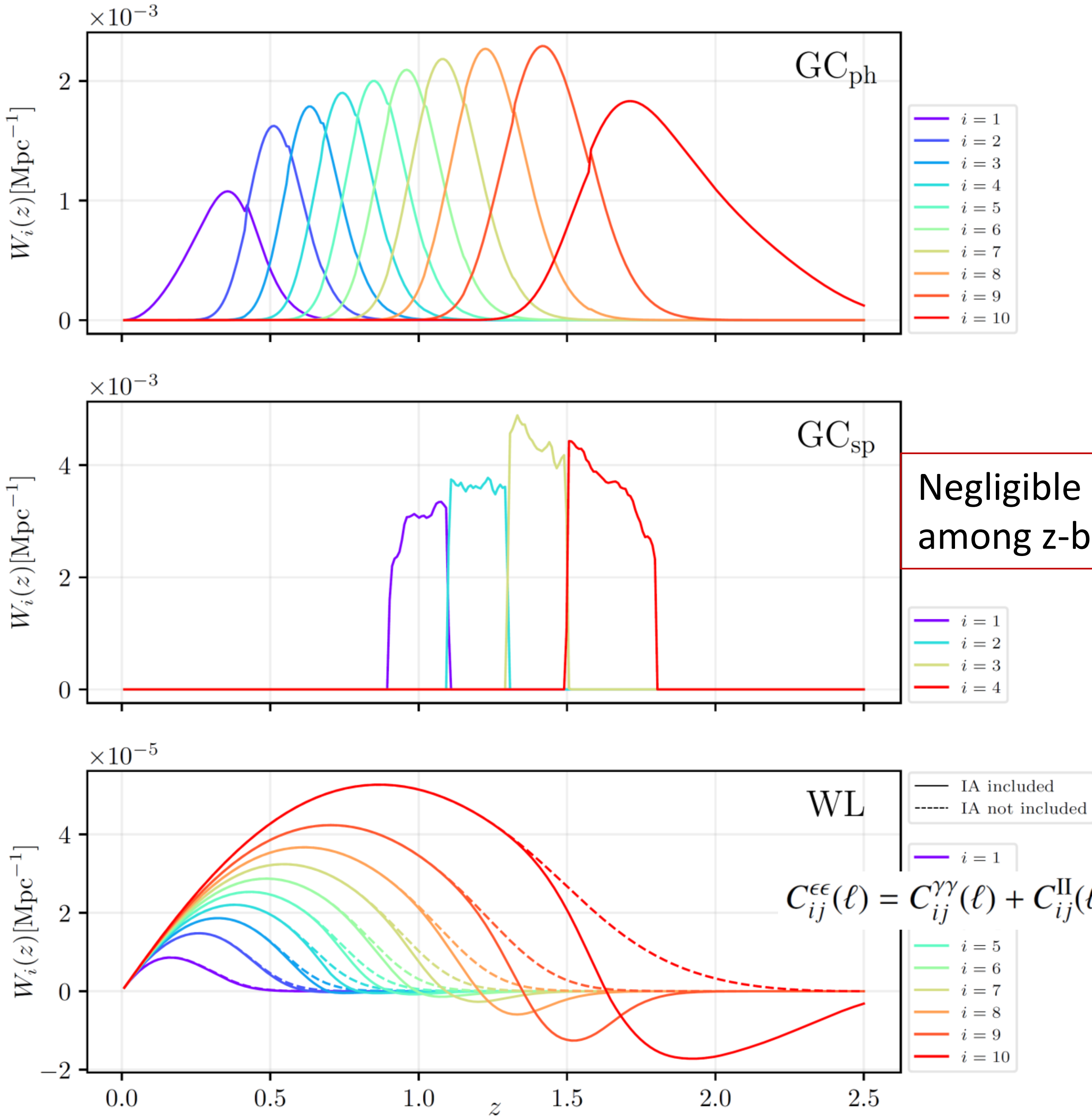

Negligible correlations among z-bins

$$C_{ij}^{\epsilon\epsilon}(\ell) = C_{ij}^{\gamma\gamma}(\ell) + C_{ij}^{\mathrm{II}}(\ell) + C_{ij}^{\mathrm{I}\gamma}(\ell) + N_{ij}^{\epsilon}(\ell)$$

The ΛCDM model

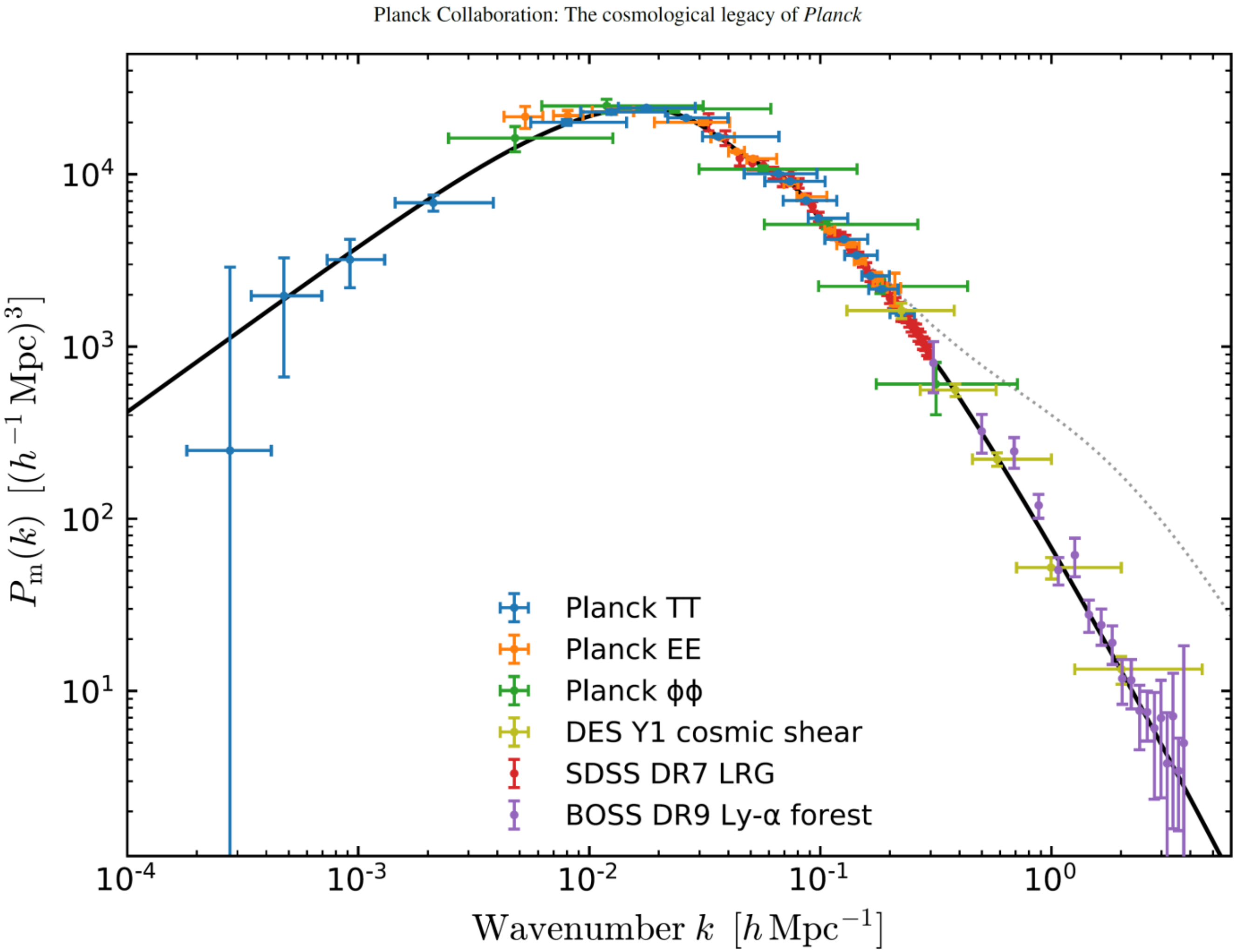

Forecasts of Euclid scientific performance

REFERENCE PAPER: Euclid Consortium, arXiv:1910.09273

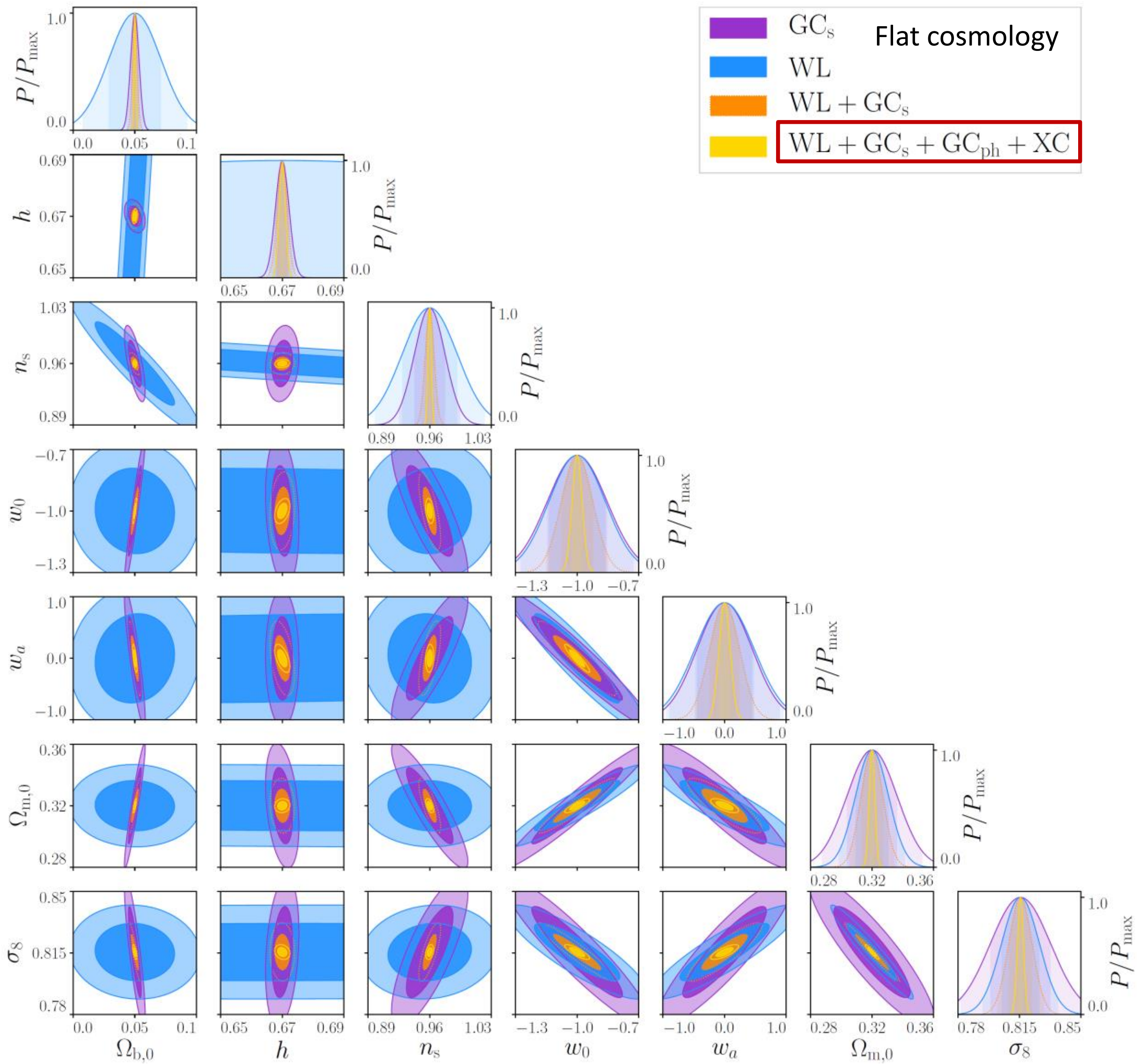

Probe combination is key to high precision and accuracy

REFERENCE PAPER: Euclid Consortium, arXiv:1910.09273

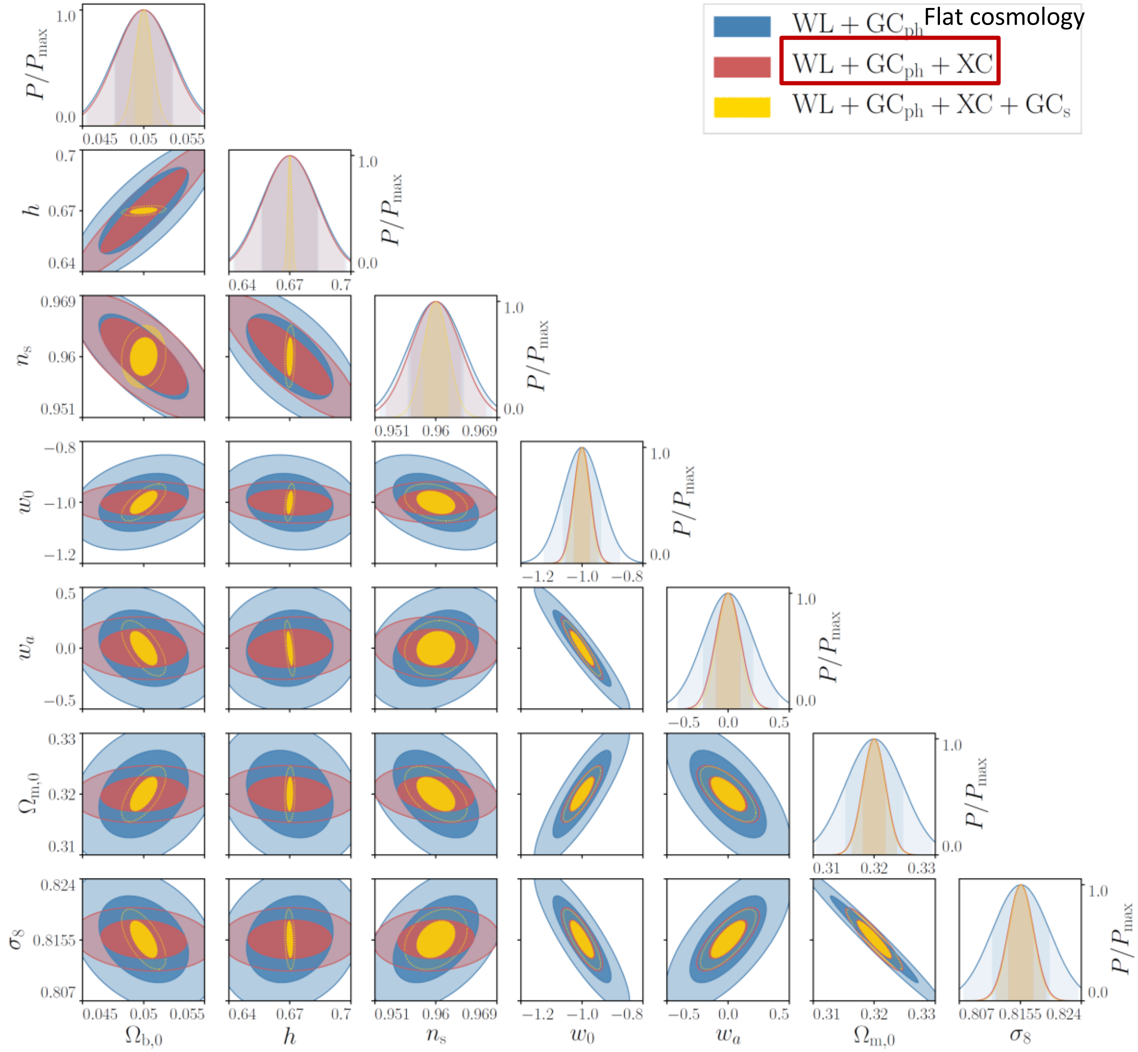

Probe combination is key to high precision and accuracy

REFERENCE PAPER: Euclid Consortium, arXiv:1910.09273

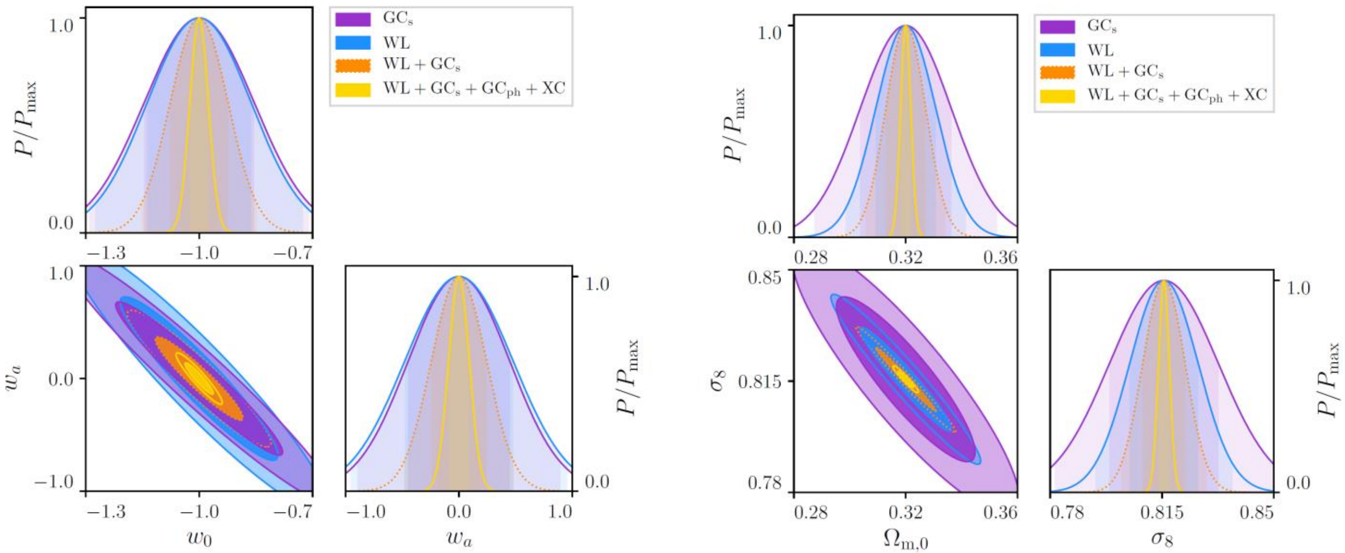

All probe combination GC_s+WL+GC_{ph}+$XC^{(GC_{ph},WL)}$								
Setting	$\Omega_{m,0}$	$\Omega_{b,0}$	$\Omega_{DE,0}$	w_0	w_a	h	n_s	σ_8
ΛCDM flat								
Pessimistic	0.0067	0.025	–	–	–	0.0036	0.0049	0.0031
Optimistic	0.0025	0.011	–	–	–	0.0011	0.0015	0.0012
w_0, w_a flat								
Pessimistic	0.0110	0.035	–	0.036	0.15	0.0053	0.0053	0.0049
Optimistic	0.0060	0.015	–	0.025	0.091	0.0015	0.0019	0.0022

Some Issues

1. Although more and more realistic, forecasts still idealised: now adding SSC and improving WL&GC_{ph} galaxy distributions, GC_{sp} purity and nonlinear modelling)

2. Yet, they focus essentially on 2-point summary statistics (so, in this respect, conservative)

3. Including more nonlinear scales gives access to extra information (e.g. higher-order), but modelling is complex

4. Likelihood computation is expensive: Deep Learning solutions

5. Covariance matrix computations (SWGs & IST:NL)

6. Investigate new probes as cosmic voids

Forecasts: adding higher-order information

$$k^B_{\rm max} = 0.08\,h\,{\rm Mpc}^{-1}$$
$$k^P_{\rm max} = 0.2\,h\,{\rm Mpc}^{-1}$$

(Moretti, Sefusatti+, in prep.)

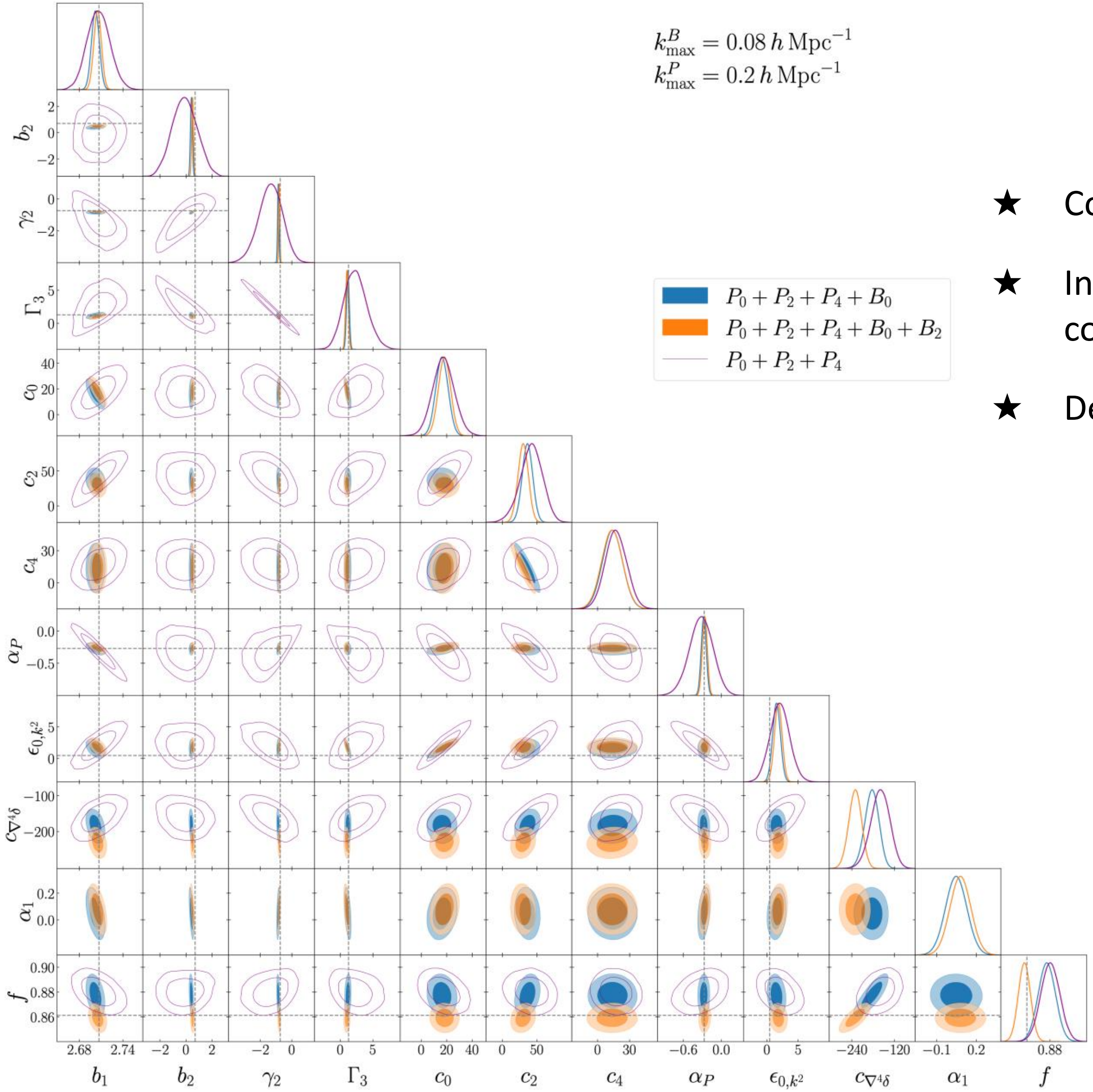

- ★ Combine P(k) and B(k)
- ★ Include redshift-space distortion constraints (multipoles)
- ★ Dedicated GC-SWG WP:HO

Speeding up the cosmological parameters inference with 2pt-emulators and differentiable likelihoods

Cosmological inference is based on Bayes Theorem:

$$P(\theta \mid D) = \frac{\mathcal{L}(D|\theta)P(\theta)}{P(D)}$$

Our goal: posterior on data

Likelihood function, connecting **theory** and **data**

Prior on model parameters

3x2pt: WL+GC$_{ph}$+X

Replace expensive computations of model power spectra with a trained neural network power spectra

- **Speed-up ~10^3**
- **Accuracy <0.2% on all scales**

$$\mathcal{L}(\boldsymbol{D} \mid \boldsymbol{\theta}) \propto \exp\left(-\tfrac{1}{2}\left[(\boldsymbol{D}-\boldsymbol{C}(\boldsymbol{\theta}))^{\mathrm{T}}\boldsymbol{Cov}^{-1}(\boldsymbol{D}-\boldsymbol{C}(\boldsymbol{\theta}))\right]\right)$$

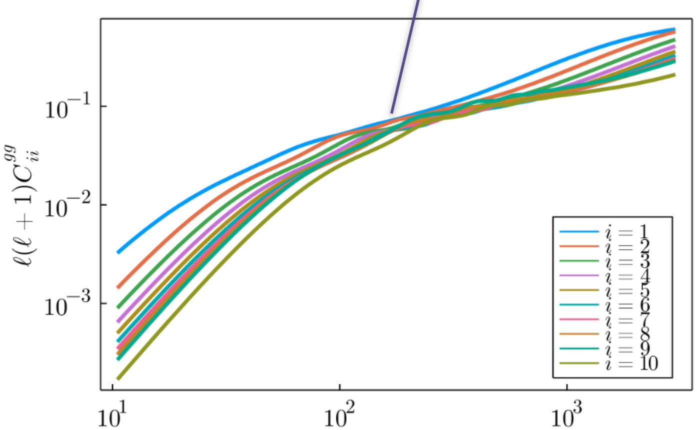

Bonici et al. 2022

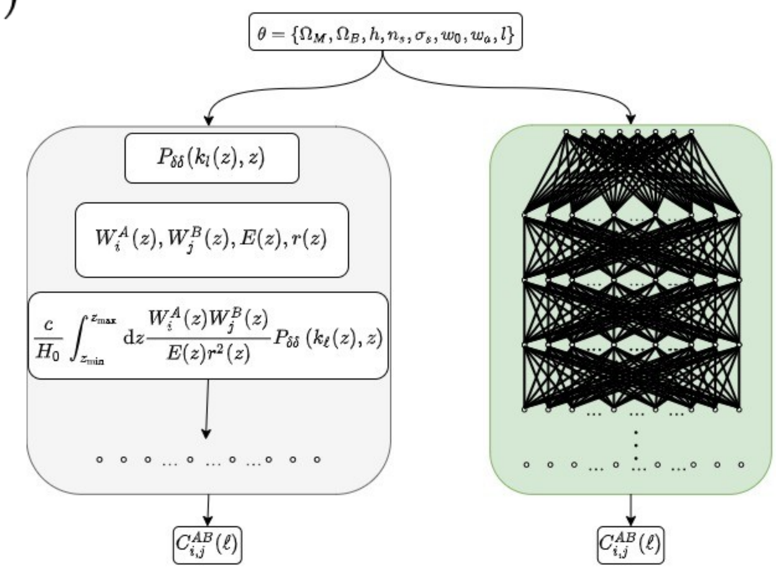

Speeding up the cosmological parameters inference with 2pt-emulators and differentiable likelihoods

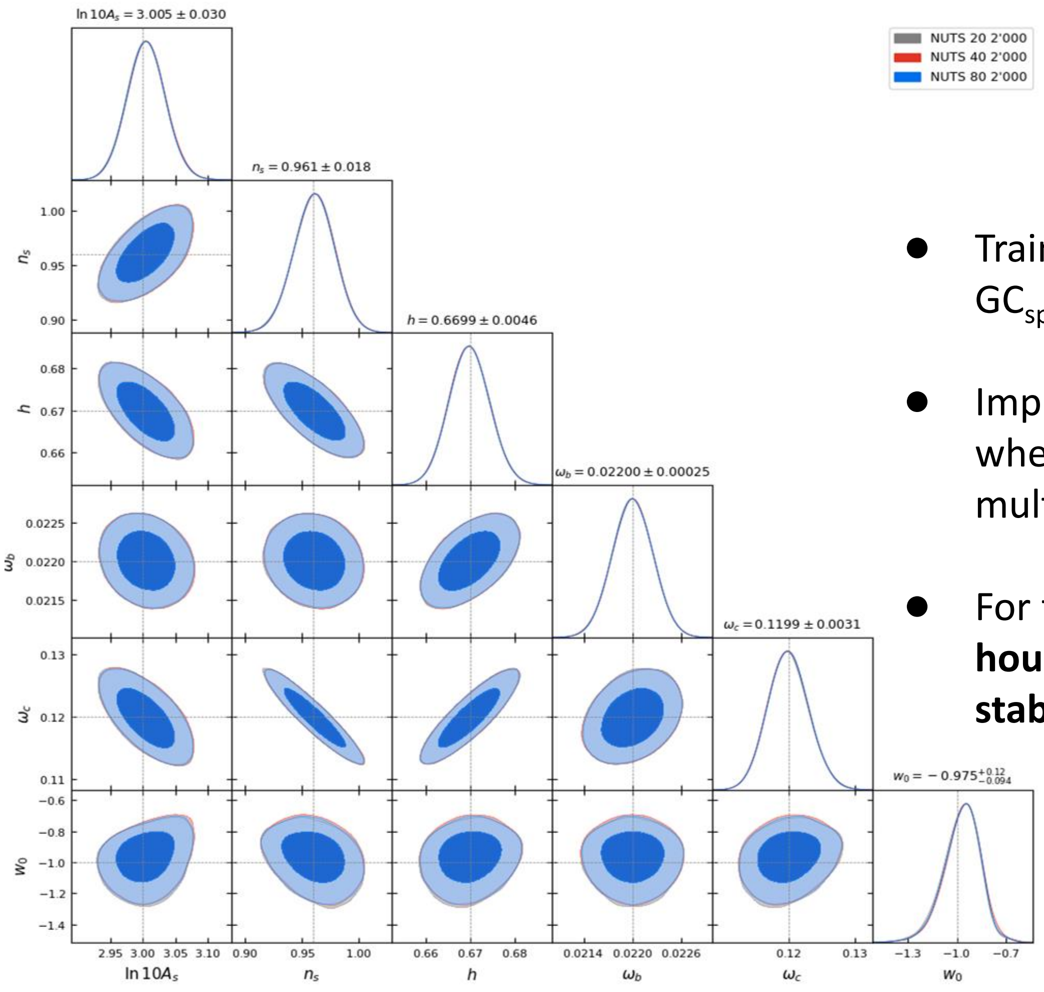

GCsp likelihood:

- Trained emulators to mimic PyBird predictions for GC_{sp} power spectra at all Euclid **spectro redshifts**
- Improved performance, the **likelihood computation** when considering 4 spectroscopic bins and 3 multipoles requires **0.5 milliseconds**
- For the full GCsp-sample the **chains run** in about **1 hour** and have shown a optimal **convergence** and **stability** using Hamiltonian MCMC.

Bonici & EC in prep. (Euclid Pre-launch Key Project GC-6 paper-3)

Don’t forget cosmic voids!
Parameter inference from photo&spectro voids

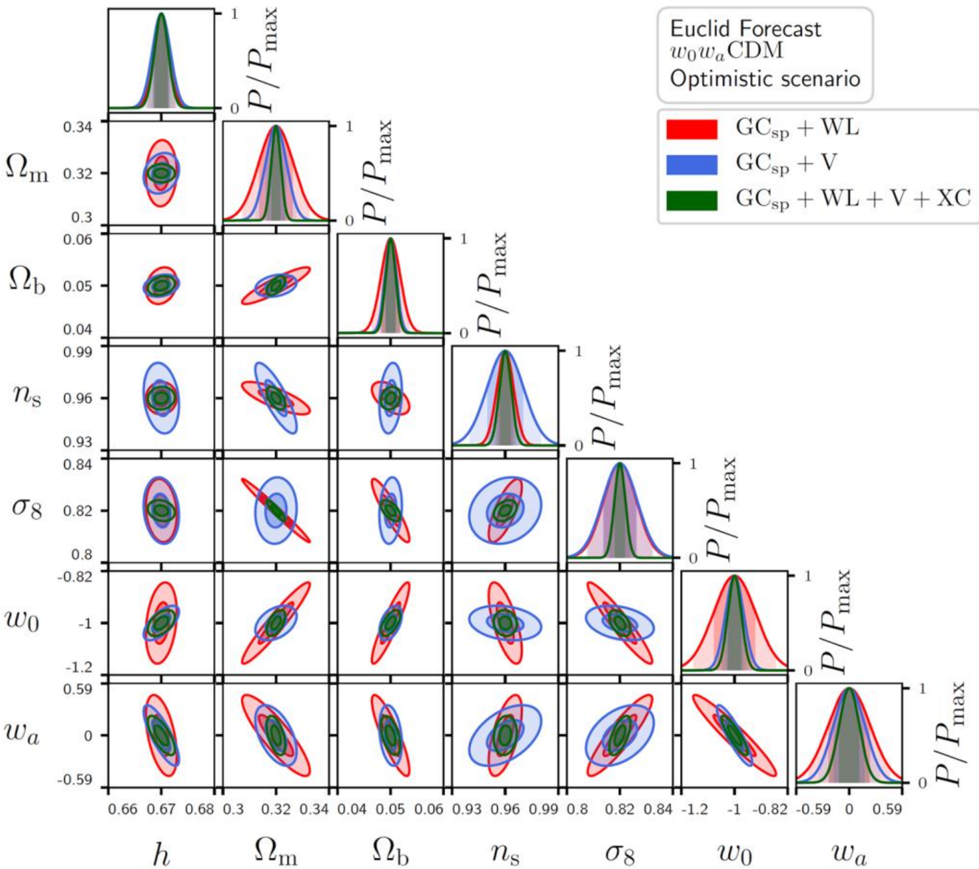

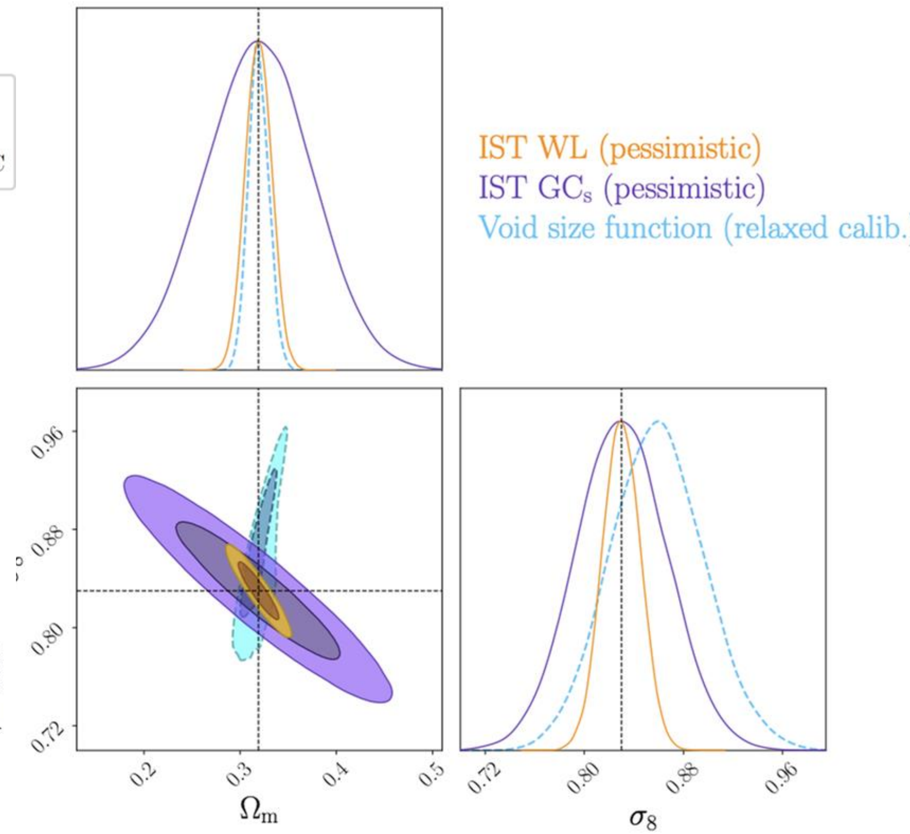

Bonici & EC 2022

Contarini & EC 2021

Stay tuned for more!